Periodic Trends and Ligand Effects on the Substitution Labilities of Tetrametal Cluster Complexes of the Cobalt Triad. Molecular Structure of $Rh_4(CO)_8\{HC[P(C_6H_5)_2]_3\}[P(OC_2H_5)_3]$

J. R. Kennedy,[1a] Peter Selz,[1a] Arnold L. Rheingold,*[1b] William C. Trogler,*[1c] and Fred Basolo*[1a]

Contribution from the Departments of Chemistry, Northwestern University, Evanston, Illinois 60201, the University of Delaware, Newark, Delaware 19716, and the University of California at San Diego, La Jolla, California 92093. *Received September 8, 1988*

Abstract: The substitution kinetics of $M_4(CO)_9[HC(PPh_2)_3]$ clusters (M = Co, Rh, and Ir) with a variety of phosphorus donor ligands, L, has been explored. In each case CO substitution occurs at the apical metal atom to form $M_4(CO)_8[HC(PPh_2)_3]L$. Crystals of $Rh_4(CO)_8[HC(PPh_2)_3][P(OEt)_3]\cdot CH_2Cl_2$ were examined by X-ray crystallography and found to belong to the monoclinic space group $P2_1/n$ with a = 14.482 (6) Å, b = 18.747 (7) Å, c = 20.92 (1) Å, β = 98.90 (3)°, V = 5611 (3) Å^3, and Z = 4. Refinement of 563 least-squares variables for 4648 unique reflections with $F_o > 4.5\sigma(F_o)$ led to R_F = 0.0636 and R_{wF} = 0.0706. The compound adopts a tetrahedral metal atom structure with three P of the $HC(PPh_2)_3$ ligand bound in axial positions. Each edge of the basal triangle of Rh atoms is bridged by a CO ligand (Rh–Rh of 2.744 (1) Å, 2.771 (2) Å, and 2.760 (2) Å). The $P(OEt)_3$ ligand substitutes on the unique apical Rh atom (Rh–P = 2.253 (5) Å). The most unusual aspect of the structure is a highly asymmetric bridging carbonyl group connecting the apical Rh atom and a basal Rh (Rh^{ap}–C = 1.77 (2) Å, Rh^{ba}–C = 2.08 (2) Å). The Rh–Rh bond between these bridged atoms of 2.923 (2) Å significantly exceeds the other Rh^{ap}–Rh^{ba} distances (2.676 (2) Å and 2.685 (2) Å). Kinetic studies for the $M_4(CO)_9[HC(PPh_2)_3]$ cluster family show that two term rate laws $(k_1 + k_2[L])[M_4(CO)_9[HC(PPh_2)_3]]$ are observed for M = Co and Rh, whereas for Ir the second-order term dominates for all L except perhaps ^{13}CO. Activation parameters for the k_1 terms ($\Delta H_1^\ddagger$ = 22 to 26 kcal/mol and $\Delta S_1^\ddagger$ = 0–23 kcal/mol) are consistent with a CO dissociative mechanism for the k_1 process. Activation parameters for the k_2 terms ($\Delta H_2^\ddagger$ = 5 to 14 kcal/mol, $\Delta S_2^\ddagger$ = −20 to −45 cal/(mol·K)) and the dependence of rate on incoming nucleophile suggest an associative mechanism for CO substitution, where L attacks an apical metal atom of the cluster. Rates of CO substitution in $M_4(CO)_9[HC(PPh_2)_3]$ are generally less than in corresponding $M_4(CO)_{12}$ clusters since the $HC(PPh_2)_3$ ligand donates electron density to the cluster (as compared to CO). This results in enhanced π-back-bonding to CO groups in the cluster (a raised barrier to CO dissociation) and a decreased susceptibility to nucleophilic attack. An anomalous high reactivity of $Ir_4(CO)_9(PPh_3)_3$ as compared to $Ir_4(CO)_9[HC(PPh_2)_3]$ is shown to arise from an enhanced rate of CO dissociation, which can be attributed to the presence of bridging CO groups in the former complex. A unique aspect of substitution in the cluster compounds as compared to mononuclear carbonyl complexes is the presence of rapid associative paths for CO substitution. This may result from the presence of low-lying acceptor orbitals for nucleophilic attack derived from metal–metal antibonding orbitals of the cluster. Periodic effects on the k_1 path follow the order of increasing reactivity Ir ≪ Co < Rh with the relative reactivities of 10^{-5}:1:667, while the k_2 path follows the order Ir < Co ≪ Rh with ratios of 10^{-3}:1:10^6. The most notable chemical feature is the exceptional reactivity of the rhodium cluster, whose substitution reactions proceed within seconds at room temperature.

Transition-metal carbonyl cluster complexes form an interesting class of compounds, whose structures, bonding, and reactivity differ significantly from mononuclear carbonyls. One key for a better understanding of reactivity in these compounds is to define factors that control ligand exchange at a single metal center imbedded in a cluster. A quantitative exploration of trends in reactivity for a series of clusters, such as $M_3(CO)_{12}$, where M = Fe, Ru, and Os, may be hampered by competing fragmentation reactions.[2] Through a series of careful studies[3a,b] the ordering of dissociative rates was shown to follow the pattern Fe > Rh ≫ Os, while associative reactions follow the trend Ru ≫ Os. A quantitative comparison of rates and mechanisms among the $M_4(CO)_{12}$ cluster family (M = Co, Rh, and Ir) has been foiled by the high reactivity of $Co_4(CO)_{12}$, which results from an autocatalytic process after an induction period,[3c] rather than from an intrinsic property of the cluster. Osborn and co-workers[4] have shown that the tripod ligand, $HC(PPh_2)_3$, stabilizes the cluster series $M_4(CO)_9[HC(PPh_2)_3]$ toward fragmentation processes. The electronic structures and physical properties of these clusters are also characterized,[5] which makes them ideal candidates for a comparative mechanistic study. Darensbourg and Zalewski[6] previously have reported rates for the reaction between $Co_4(CO)_9$(tripod) and ^{13}CO. Their work focused on dissociative loss of CO in the cluster. Herein we report results to assess periodic and structural effects on associative and dissociative rates for CO substitution in tetrametal tripod clusters of Co, Rh, and Ir (Figure 1). A remarkably rapid associative mechanism for CO displacement was observed in $Rh_4(CO)_9$(tripod).

Experimental Section

Dichloromethane was dried over and distilled from phosphorus pentoxide. Hexane and pentane were washed with sulfuric acid, predried over sodium hydroxide, and distilled from sodium benzophenone ketyl. Dimethoxyethane (DME) and tetrahydrofuran (THF) were dried over and distilled from sodium benzophenone ketyl. Chlorobenzene was washed with H_2SO_4, saturated aqueous sodium bicarbonate, and water, predried over calcium chloride, and distilled from P_2O_5. Deuteriated dichloromethane was degassed (3 freeze–pump–thaw cycles) and stored over P_2O_5. It was vacuum transferred to the reaction vessel before use. The

(1) (a) Northwestern University. (b) University of Delaware. (c) University of California at San Diego.
(2) Bruce, M. I. *Coord. Chem. Rev.* **1987**, *76*, 1.
(3) (a) Shojaie, A.; Atwood, J. D. *Organometallics* **1985**, *4*, 187. (b) Poë, A. J.; Sekhar, V. C. *Inorg. Chem.* **1985**, *24*, 4376. (c) Kennedy, J. R.; Basolo, F.; Trogler, W. C. *Inorg. Chim. Acta* **1988**, *146*, 75.
(4) (a) Arduini, A. A.; Bahsoun, A. A.; Osborn, J. A.; Voelker, C. *Angew. Chem., Int. Ed. Engl.* **1980**, *19*, 1024. (b) Bahsoun, A. A.; Osborn, J. A.; Voelker, C.; Bonnet, J. J.; Lavigne, G. *Organometallics* **1982**, *1*, 1114. (c) Bahsoun, A. A.; Osborn, J. A.; Kintzinger, J.-P.; Bird, P. H.; Siriwardane, U. *Nouv. J. Chim.* **1984**, *8*, 125.
(5) Holland, G. F.; Ellis, D. E.; Trogler, W. C. *J. Am. Chem. Soc.* **1986**, *108*, 1884. Holland, G. F.; Ellis, D. E.; Tyler, D. R.; Gray, H. B.; Trogler, W. C. *Ibid.* **1987**, *109*, 4276.
(6) (a) Darensbourg, D. J.; Zalewski, D. J. *Organometallics* **1985**, *4*, 92. (b) Darensbourg, D. J.; Zalewski, D. J.; Delord, T. J. *Organometallics* **1984**, *3*, 1210.

0002-7863/89/1511-3615$01.50/0

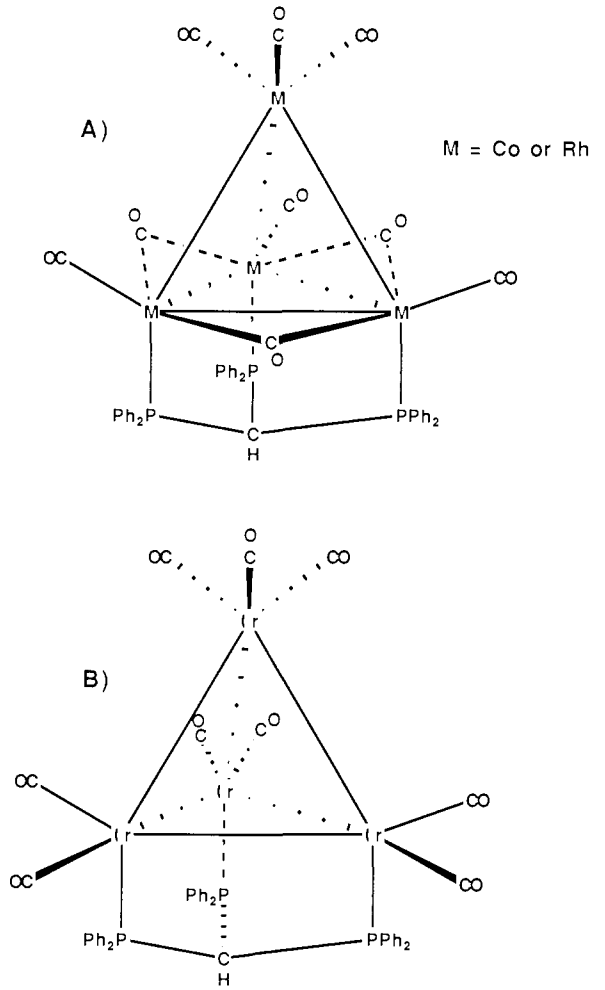

Figure 1. Structures of tripod carbonyl complexes of Co, Rh, and Ir. (a) C_{3v} structure adopted by $Co_4(CO)_9[HC(PPh_2)_3]$ and $Rh_4(CO)_9[HC(PPh_2)_3]$ with three carbonyl groups bridging the metal–metal bonds in the basal plane. (b) C_{3v} structure adopted by $Ir_4(CO)_9[HC(PPh_2)_3]$, which contains only terminal carbonyls.

deuteriated toluene solvent was heated with molten sodium, degassed, and vacuum distilled.

Tris(diphenylphosphino)methane ($HC(PPh_2)_3$ or tripod) was purchased from (Aldrich) and used without purification. Triphenylphosphine (PPh_3) and triphenylarsine ($AsPh_3$) were purchased from (Strem) and recrystallized from ethanol. All liquid phosphines (PR_3) or phosphites ($P(OR)_3$) were purchased (Strem) and distilled from molten sodium. Carbon-13 labeled carbon monoxide (^{13}CO, 99%) was purchased (Monsanto). Rhodium trichloride trihydrate was obtained on loan (Johnson-Matthey). Octacarbonyldicobalt was purchased (Strem) and stored cold under an N_2 atmosphere.

All NMR spectra were recorded with use of a JEOL FX-90Q, a JEOL FX-270, or a Varian XLA-400 spectrometer. All IR spectra were recorded on either a Perkin-Elmer Model 283 spectrophotometer or a Nicolet 170-FX Fourier transform spectrometer. Chemical shifts are referenced to 85% H_3PO_4 (external reference) for ^{31}P NMR and to TMS for ^{13}C NMR spectra. Positive shifts are downfield. The IR spectra are reported for the carbonyl stretching region. All electronic spectra were recorded on either Perkin-Elmer Model 330 or 320 spectrophotometers. The variable-temperature IR cell was a SPECAC Model P/N 21.000 employing a 0.5 mm pathlength cell, CaF_2 cell windows, AgCl outer jacket windows, and a copper–constantan thermocouple. The stopped flow apparatus was a modified Applied Photophysics (London) Model 1705 instrument with a 2 cm pathlength quartz cell. The stopped flow spectrometer was interfaced to an Apple II Plus computer for data collection. The analog to digital converter, timing board (clock), collection board, and software were purchased from Interactive Microware. Liquid circulating constant temperature baths used were either NESLAB Model RTE-8 or various Haake models.

$Ir_4(CO)_9[HC(PPh_2)_3]$. This cluster was prepared by "method" 1 of a previously reported synthesis.[4b] IR, ν(CO) region (cm^{-1}, CH_2Cl): 2064 (m), 2011 (s), 1979 (vw), 1954 (w) (obsd); 2060 (s), 2010 (vs), 1978 (w), 1951 (m) (lit.).[4a] $^{31}P\{^1H\}$ NMR (CD_2Cl_2): δ −39.1 (s) (obsd); −39.1 (s) (lit.).[4b]

Table I. $^{31}P\{^1H\}$ NMR Data for $Rh_4(CO)_8[HC(PPh_2)_3]L$ Clusters at 25 °C

L	solvent	δ,[a] ppm	coupling constants, Hz $^1J_{P-Rh}$	$^3J_{P-P}$
CO[b]	CD_2Cl_2	18.0 (m), 14.4 (d, m)	133	
CO	acetone-d_6	15.9 (d, m)	139	
$P(OMe)_3$	CD_2Cl_2	A 133.5 (d, q)	222	113
		B 14.0 (d, d, m)	~114	113
$P(OEt)_3$	CD_2Cl_2	A 126.9 (d, q)	220	110
		B 14.2 (d, d, m)	~110	110
$P(OMe)_2Ph$	CD_2Cl_2	A 150.8 (d, q)	183	94
		B 13.5 (d, d, m)	113	94
$P(O\text{-}i\text{-}Pr)_3$	CD_2Cl_2	A 125.2 (d, q)	230	102
		B 15.4 (d, d, m)	~103	102
	THF-d_8	A 127.6 (d, q)	232	104
		B 15.9 (d, d, m)	~105	104
PPh_3	CD_2Cl_2	A 26.1 (d, q)	146.5	61.0
		B 16.0 (d, d, m)	~80	61.0
	THF-d_8	A 26.7 (d, q)	146.5	61.0
		B 16.4 (d, d, m)	~80	61.0
PPh_3[c]	CD_2Cl_2	A 25.0 (m)		
		B 15.1 (m)		
$PPh_2C_2H_4$-$Si(OEt)_3$[c]	CD_2Cl_2	A 23.9 (m)		
		A 13.4 (m)		

[a] A = phosphorus ligand, L; B = $HC(PPh_2)_3$. Chemical shifts, δ, are positive downfield to 85% H_3PO_4 (ext. ref.), multiplicity of signal given in parentheses; s = singlet, d = doublet, t = triplet, q = quartet, m = multiplet. [b] Reference 4b. [c] Reference 7.

$Rh_4(CO)_9[HC(PPh_2)_3]$. This cluster was prepared by a literature method[4b] and purified by recrystallization (saturated CH_2Cl_2 solution with careful addition of hexane followed by cooling for several days) following chromatography on silica gel with CH_2Cl_2 as eluent. IR, ν(CO) (cm^{-1}, CH_2Cl_2): 2059 (s), 2010 (vs), 1990 (sh), 1840 (w, sh), 1803 (m) (obsd); 2060 (s), 2010 (vs), 1990 (sh), 1840 (w, sh), 1803 (m) (lit.).[4b] $^{31}P\{^1H\}$ NMR (CD_2Cl_2): δ 19 (m), 14.8 (m, $^1J_{Rh-P}$ = 132 Hz) (obsd); 18.0 (m), 14.4 (m, $^1J_{Rh-P}$ = 133 Hz) (lit.).[4b]

$Co_4(CO)_9[HC(PPh_2)_3]$. This compound was prepared according to a published procedure.[4b] Chromatography on silica gel with CH_2Cl_2 as eluent followed by recrystallization (saturated CH_2Cl_2 solution with careful addition of hexane and cooling for several days) gave pure material. IR, ν(CO) (cm^{-1}, CH_2Cl_2): 2050 (s), 2000 (vs), 1975 (sh), 1780 (m) (obsd); 2050 (s), 2000 (s), 1975 (sh), 1780 (m) (lit.).[4b]

$Co_4(CO)_8[HC(PPh_2)_3]L$ (L = $P(n\text{-}Bu)_3$, $P(Me)_3$). These species were not isolated. IR spectra of solutions of these compounds were identical with previously isolated and characterized analogues[4b,6] (Supplementary Table I).

$Rh_4(CO)_8[HC(PPh_2)_3]L$ (L = $P(OEt)_3$, $P(O\text{-}i\text{-}Pr)_3$, PPh_3, $P(n\text{-}Bu)_3$, $P(OMe)_3$). The method is similar for all compounds and the procedure for L = $P(OEt)_3$ will be given. A solution of $Rh_4(CO)_9[HC(PPh_2)_3]$ was prepared by dissolving 80.0 mg (6.49×10^{-2} mmol) in 20.0 mL of CH_2Cl_2 or THF. To this solution 1.0 mL of a 6.5×10^{-2} M solution of $P(OEt)_3$ in CH_2Cl_2 or THF was added with stirring at room temperature. The solution immediately deepens in color from red to dark purple red and the IR spectrum shows an absence of starting material. The solution was stirred for an additional 15 min. On reducing the volume to about 7 mL, addition of an equivalent volume of hexane, followed by cooling to 0 °C, precipitated dark purple microcrystalline product. This product was filtered and washed with hexane (3×). Recrystallization from a minimum amount of CH_2Cl_2 or THF and careful addition of hexane (to effect slow diffusion of hexane into the solution) followed by cooling to −30 °C for several days yields large plate-like crystals. These crystals were suitable for X-ray crystal structure analysis. Isolated yields are good (>60%). IR data for the $Rh_4(CO)_8[HC(PPh_2)_3]L$ clusters are given in Supplementary Table II. $^{31}P\{^1H\}$ NMR data are given in Table I, and visible absorption spectra are given in Supplementary Table III.

$Ir_4(CO)_8[HC(PPh_2)_3]L$ (L = $P(n\text{-}Bu)_3$, $P(OMe)_3$). These clusters were prepared in solution with use of a large excess of ligand and temperatures between 30 and 80 °C. Their IR and ^{31}P NMR spectra were compared to previously published data[7] (Supplementary Table IV).

$Rh_4(CO)_7[HC(PPh_2)_3]L_2$ (L = $P(O\text{-}i\text{-}Pr)_3$, $P(OEt)_3$, $P(n\text{-}Bu)_3$). These clusters were prepared by a method similar to the $Rh_4(CO)_8$-

(7) Foster, D. F.; Harrison, J.; Nicholls, B. S.; Smith, A. K. *J. Organomet. Chem.* **1983**, *248*, C29.

Table II. $^{31}P\{^1H\}$ NMR Data for $Rh_4(CO)_7[HC(PPh_2)_3]L_2$ Clusters at 25 °C

L	solvent	isomer[a]	phosphorus center[b]	δ,[c] ppm	coupling constants, Hz $^1J_{P-Rh}$	coupling constants, Hz $^3J_{P-P}$
$P(OMe)_3$	CD_2Cl_2	A	$L_AL_{A'}$	135.7 (dq)	224	110
			$P_AP_{A'}P_{A''}$	12.9 (dt)	~107	110
$P(OMe)_2Ph$	CD_2Cl_2	A	$L_AL_{A'}$	156.5 (dq)	220	79
			$P_AP_{A'}P_{A''}$	14.7 (dt)	~87	79
$P(O\text{-}i\text{-}Pr)_3$	CD_2Cl_2	A	$L_AL_{A'}$	126.3 (dq)	232	100
			$P_AP_{A'}P_{A''}$	17.3 (m)		
$P(OEt)_3$	CD_2Cl_2	B	L_A	~130 (m)		
			L_B	124.8 (ddm)	275	34
			$P_AP_{A'}$	20.6 (m)		
			P_B	17.2 (m)		
$P(OMe)_2Ph$	CD_2Cl_2	B	L_A	~148 (m)		
			L_B	161.7 (dm)	223	
$P(O\text{-}i\text{-}Pr)_3$	CD_2Cl_2	B	L_A	129.7 (dtd)	247	93
						71
			L_B	136.2 (dm)	271	
			$P_AP_{A'}$	24.6 (m)		
			P_B	18.2 (m)		
$P(O\text{-}i\text{-}Pr)_3$	THF-d_8	B	L_A	132 (dtd)	250	98
						55
			L_B	138 (dm)	270	
			$P_AP_{A'}$	26 (m)		
			P_B	19 (m)		

[a] Isomer A = apical-apical, see Figure 7; isomer B = apical-basal, see Figure 7. [b] Refer to Figure 7 for phosphorus atom position. [c] Chemical shifts, δ, are positive to 85% H_3PO_4 (ext. ref.). Multiplicity of the signal given in parentheses; s = singlet, d = doublet, t = triplet, q = quartet, m = multiplet.

Table III. Crystal and Data Collection Parameters for $C_{51}H_{46}O_{11}P_4Rh_4{\cdot}CH_2Cl_2$

		(a) Crystal Parameters	
crystal size, mm	0.27 × 0.27 × 0.27	V, Å^3	5611 (3)
crystal system	monoclinic	Z	4
space group	$P2_1/n$	d_{calc}, g cm^{-3}	1.72
a, Å	14.482 (6)	μ, cm^{-1}	13.9
b, Å	18.747 (7)	temp. °C	24
c, Å	20.92 (1)	formula wt	1455.4
β, deg	98.90 (3)		
		(b) Data Collection Parameters	
diffractometer	Nicolet R3m/μ	scan speed, deg min^{-1}	variable, 5–20
radiation	Mo Kα	data collected	$\pm h$, $+k$, $+l$
monochromator	graphite	indpdt data	7778 (8318 read)
scan technique	Wyckoff	indpdt data, $F_o \geq 4.5\sigma(F_o)$	4648
2θ scan range, deg	4–46	std rflns	3 std/197 rflns
		(c) Refinement	
R_F, %	6.36	Δ/σ	0.059
R_{wF}, %	7.06	$\Delta\rho$, e Å^{-3}	1.21 (near Rh(1))
GOF	1.13	LS params	563

$[HC(PPh_2)_3]L$ clusters. To a 25-mL, stirred, 6.62 × 10^{-3} M CH_2Cl_2 or THF solution of $Rh_4(CO)_9[HC(PPh_2)_3]$ was added 1.5 mL of a 0.23 M solution of $P(OEt)_3$. On addition, there was an immediate color change from red to dark red/purple. An IR spectrum of this solution showed that it contained mostly $Rh_4(CO)_9[HC(PPh_2)_3][P(OEt)_3]$. The solution was stirred for about 3 days at room temperature during which time occasional samples were removed and IR and $^{31}P\{^1H\}$ NMR spectra recorded. After observing that all the $Rh_4(CO)_8[HC(PPh_2)_3][P(OEt)_3]$ had reacted, 40 mL of hexane was added to the solution and a dark purple solid precipitated. This was filtered and washed with hexane (3 × 10 mL). The solid was then dissolved in CH_2Cl_2 and chromatographed with silica gel as the solid support and CH_2Cl_2 as eluent. The purple fraction was collected, reduced in volume, carefully diluted with hexane, and cooled to 30 °C for several days. Solid product always formed but crystalline material suitable for X-ray analysis was not obtained. Depending on the ligand, one of two isomers was formed as seen in the $^{31}P\{^1H\}$ NMR spectra (Table II). The IR data are reported in Supplementary Table V.

Kinetic Methods. Methods of the rate measurements and data reduction were similar to those used previously.[3]

X-ray Structure Determination of $Rh_4(CO)_8[HC(PPh_2)_3][P(OEt)_3]$. Crystal data and parameters for collection and refinement of data are contained in Table III. A deep red crystal of $C_{51}H_{46}O_{11}P_4Rh_4{\cdot}CH_2Cl_2$, grown from CH_2Cl_2, was mounted with epoxy on a glass fiber. On the basis of systematic absences the space group was determined as monoclinic $P2_1/n$. Unit-cell dimensions were derived from the least-squares fit of the angular settings of 25 reflections with $20° < 2\theta < 25°$. Data were corrected for absorption effects with a program based on deviations between F_o and F_c (XABS, H. Hope).

The structure was solved by direct methods (SOLV), which located the four rhodium atoms. The remaining non-hydrogen atoms were located from subsequent difference Fourier syntheses and refined anisotropically. Hydrogen atoms were calculated and fixed in idealized positions (d(C–C) = 0.96 Å, U = 1.2 times the isotropic equivalent for the carbon atom to which it was attached). All phenyl rings were constrained to rigid planar hexagons. Ethoxy carbon–carbon distances, which showed signs of disorder, were tied to a common variable that refined to 1.40 (2) Å. One molecule of $C_{51}H_{46}O_{11}P_4Rh_4$ and one molecule of CH_2Cl_2 crystallize per asymmetric unit.

An inspection of F_o vs F_c values and trends based upon sin θ, Miller index, or parity group showed no systematic errors in the data. All computer programs used in the data collection and refinement are contained in the Nicolet program packages P3, SHELXTL (version 5.1) and XP (Nicolet XRD, Madison, WI). Atomic coordinates are provided in Table IV, selected bond distances in Table V, and selected bond angles in Table VI. Complete tables of crystallographic data are provided as supplementary material.

Results

Reaction between $Co_4(CO)_9[HC(PPh_2)_3]$ and Ligand L. The reaction between $Co_4(CO)_9[HC(PPh_2)_3]$ and excess $P(n\text{-}Bu)_3$ or $P(OMe)_3$ proceeds directly and quantitatively to $Co_4(CO)_8[HC$-

Table IV. Atomic Coordinates ($\times 10^4$) and Isotropic Thermal Parameters (10^3 Å^2) for $C_{51}H_{46}O_{11}P_4Rh_4 \cdot CH_2Cl_2$ (1)

	x	y	z	U[a]		x	y	z	U[a]
Rh(1)	4759.0 (8)	629.7 (7)	1621.3 (6)	56.2 (5)	C(21)	4390 (7)	2499 (4)	4070 (5)	57 (6)
Rh(2)	4879.2 (7)	2026.8 (6)	1880.5 (5)	41.1 (4)	C(22)	4798	2877	4616	69 (7)
Rh(3)	3893.2 (8)	1246.6 (6)	2666.9 (5)	44.5 (4)	C(23)	4589	3597	4680	70 (7)
Rh(4)	3201.8 (7)	1423.2 (6)	1365.7 (5)	42.1 (4)	C(24)	3972	3940	4198	65 (7)
P(1)	3163 (2)	2316 (2)	2919 (2)	38 (1)	C(25)	3565	3562	3652	50 (6)
P(2)	4184 (2)	3127 (2)	1990 (2)	38 (1)	C(26)	3774	2842	3588	48 (5)
P(3)	2311 (2)	2437 (2)	1506 (2)	38 (1)	C(31)	1616 (7)	1513 (5)	3134 (4)	49 (5)
P(4)	6294 (3)	367 (3)	1747 (2)	81 (2)	C(32)	809	1367	3398	74 (7)
Cl(1)	8689 (10)	4241 (6)	939 (7)	255 (8)	C(33)	430	1886	3758	65 (6)
Cl(2)	7363 (11)	3449 (7)	152 (7)	303 (9)	C(34)	857	2552	3855	85 (8)
Cs	8369 (30)	3565 (18)	498 (20)	306 (30)	C(35)	1664	2699	3591	57 (6)
C(1)	4254 (16)	−172 (12)	1144 (12)	113 (11)	C(36)	2044	2180	3231	59 (6)
O(1)	3947 (17)	−657 (9)	883 (10)	197 (12)	C(41)	5537 (6)	3504 (4)	3028 (5)	54 (6)
C(2)	6078 (12)	2307 (10)	1805 (8)	71 (7)	C(42)	6021	3969	3483	79 (8)
O(2)	6836 (9)	2536 (8)	1782 (8)	110 (7)	C(43)	5761	4685	3490	75 (8)
C(3)	3805 (11)	799 (9)	3458 (9)	66 (7)	C(44)	5018	4936	3042	67 (7)
O(3)	3758 (11)	521 (7)	3946 (7)	105 (7)	C(45)	4534	4472	2588	59 (6)
C(4)	2529 (13)	1050 (9)	593 (8)	68 (7)	C(46)	4794	3756	2581	39 (5)
O(4)	2127 (11)	767 (8)	149 (7)	115 (7)	C(51)	3340 (6)	4252 (5)	1189 (4)	47 (5)
C(5)	4569 (14)	338 (11)	2401 (11)	111 (9)	C(52)	3292	4711	660	60 (6)
O(5)	4678 (2)	−298 (9)	2701 (8)	126 (8)	C(53)	3905	4623	213	80 (8)
C(6)	5283 (10)	1698 (8)	2814 (7)	46 (6)	C(54)	4566	4076	296	77 (8)
O(6)	5910 (7)	1676 (6)	3229 (5)	65 (4)	C(55)	4614	3617	825	58 (6)
C(7)	4358 (10)	1817 (8)	917 (8)	52 (6)	C(56)	4001	3705	1272	44 (5)
O(7)	4516 (8)	1871 (6)	395 (5)	70 (5)	C(61)	1328 (6)	3572 (5)	791 (4)	59 (6)
C(8)	2748 (10)	777 (9)	1999 (7)	55 (6)	C(62)	1042	3958	224	66 (6)
O(8)	2238 (8)	283 (6)	2044 (5)	79 (5)	C(63)	1413	3799	−335	68 (7)
C(9)	2982 (8)	2954 (7)	2201 (6)	35 (4)	C(64)	2071	3255	−329	62 (7)
O(9)	6830 (8)	499 (7)	2456 (6)	93 (6)	C(65)	2357	2869	237	51 (6)
O(10)	6648 (10)	−386 (8)	1578 (8)	129 (8)	C(66)	1986	3028	797	47 (5)
O(11)	6952 (9)	796 (11)	1333 (7)	136 (8)	C(71)	722 (6)	2840 (5)	2063 (5)	59 (6)
C(10)	7751 (20)	450 (17)	2669 (10)	176 (17)	C(72)	−221	2773	2122	78 (8)
C(11)	8112 (20)	636 (20)	3230 (15)	257 (29)	C(73)	−742	2202	1829	78 (7)
C(12)	6281 (20)	−934 (13)	1781 (15)	148 (15)	C(74)	−320	1698	1478	76 (7)
C(13)	6521 (16)	−1632 (13)	1380 (14)	168 (16)	C(75)	623	1765	1419	56 (6)
C(14)	6717 (17)	837 (14)	653 (9)	113 (11)	C(76)	1144	2336	1711	47 (5)
C(15)	7299 (20)	1323 (18)	419 (13)	215 (23)					

[a] Equivalent isotropic U defined as one-third of the trace of the orthogonalized U_{ij} tensor.

Table V. Selected Bond Lengths (Å) for $C_{51}H_{46}O_{11}P_4Rh_4 \cdot CH_2Cl_2$

Rh(1)–Rh(2)	2.676 (2)	Rh(4)–P(3)	2.342 (4)	Rh(3)–C(6)	2.16 (1)
Rh(1)–Rh(3)	2.923 (2)	Rh(1)–C(1)	1.89 (2)	Rh(3)–C(8)	2.19 (1)
Rh(1)–Rh(4)	2.685 (2)	Rh(1)–C(5)	1.77 (2)	Rh(4)–C(4)	1.89 (2)
Rh(2)–Rh(3)	2.760 (2)	Rh(2)–C(2)	1.84 (2)	Rh(4)–C(7)	2.17 (2)
Rh(2)–Rh(4)	2.744 (1)	Rh(2)–C(6)	2.05 (1)	Rh(4)–C(8)	1.98 (2)
Rh(3)–Rh(4)	2.771 (2)	Rh(2)–C(7)	2.08 (1)	P(1)–C(9)	1.91 (1)
Rh(1)–P(4)	2.253 (5)	Rh(3)–C(3)	1.87 (2)	P(2)–C(9)	1.89 (1)
Rh(2)–P(2)	2.323 (4)	Rh(3)–C(5)	2.08 (2)	P(3)–C(9)	1.89 (1)
Rh(3)–P(1)	2.365 (4)				

$(PPh_2)_3][P(n\text{-}Bu)_3]$ or $Co_4(CO)_8[HC(PPh_2)_3][P(OMe)_3]$, respectively (eq 1). The observation of isosbestic points during the

$$Co_4(CO)_9[HC(PPh_2)_3] + L \rightarrow Co_4(CO)_8[HC(PPh_2)_3]L + CO \quad (1)$$

$$L = P(OMe)_3,\ P(n\text{-}Bu)_3$$

reaction suggests a clean stoichiometry for the reaction. In DME solvent the substitution reaction (eq 1) obeys a two-term rate law (eq 2). This can be seen from plots of k_{obs} vs ligand concentration

$$-d[Co_4(CO)_9(HC(PPh_2)_3)]/dt = (k_1 + k_2[L])[Co_4(CO)_9(HC(PPh_2)_3)] \quad (2)$$

(Figure 2, L = $P(OMe)_3$, $P(n\text{-}Bu)_3$ at 41 °C) where the non-zero intercept gives k_1 and the non-zero slope gives k_2. For the reaction between $P(OMe)_3$ and $Co_4(CO)_9[HC(PPh_2)_3]$ (eq 1, Figure 2) at 41 °C the values of k_1 and k_2 were calculated to be 5.09×10^{-4} s^{-1} and 5.15×10^{-3} M^{-1} s^{-1} (Table VII and VIII). At 41 °C, k_1 and k_2 were found to be 6.68×10^{-4} s^{-1} and 1.05×10^{-2} M^{-1} s^{-1}, respectively, when $P(n\text{-}Bu)_3$ is the substituting ligand (eq 1). The structures of the monosubstituted clusters have L occupying an apical site of the cluster (Figure 3). This is clear from the spectroscopic (IR, NMR) data and the analogy to the $Co_4(CO)_8[HC(PPh_2)_3](PMe_3)$ derivative, whose structure has been defined crystallographically.[8]

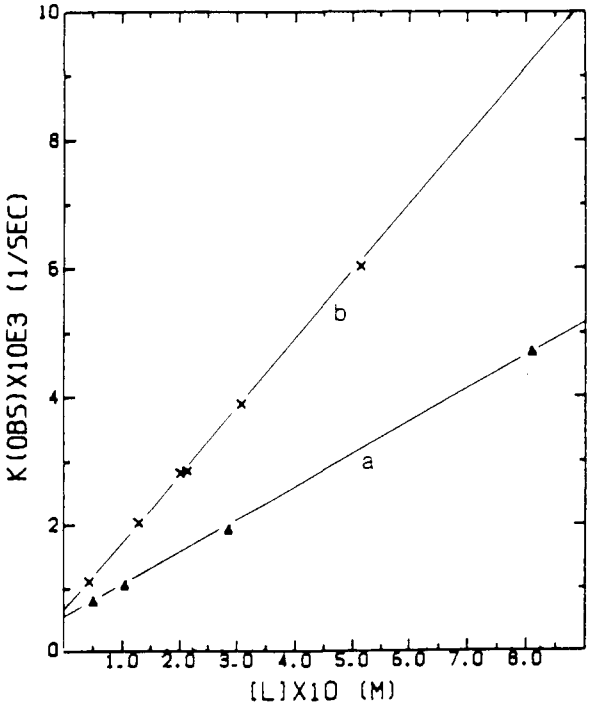

Figure 2. Plots of k_{obs} (s^{-1}) vs [L] for the reaction between $Co_4(CO)_9[HC(PPh_2)_3]$ and [L] in DME at 41 °C: (a) L = $P(OMe)_3$; (b) L = $P(n\text{-}Bu)_3$.

Table VI. Selected Bond Angles (deg) for $C_{51}H_{46}O_{11}P_4Rh_4 \cdot CH_2Cl_2$

Rh(2)-Rh(1)-Rh(3)	58.9 (1)	Rh(2)-Rh(3)-C(8)	104.1 (4)
Rh(2)-Rh(1)-Rh(4)	61.6 (1)	Rh(4)-Rh(3)-C(8)	45.2 (4)
Rh(3)-Rh(1)-Rh(4)	59.0 (1)	P(1)-Rh(3)-C(8)	99.3 (4)
Rh(2)-Rh(1)-P(4)	99.1 (2)	C(3)-Rh(3)-C(8)	103.6 (6)
Rh(3)-Rh(1)-P(4)	122.0 (1)	C(5)-Rh(3)-C(8)	80.9 (7)
Rh(4)-Rh(1)-P(4)	158.1 (2)	C(6)-Rh(3)-C(8)	148.0 (6)
Rh(2)-Rh(1)-C(1)	153.4 (7)	Rh(1)-Rh(4)-Rh(2)	59.0 (1)
Rh(3)-Rh(1)-C(1)	122.6 (8)	Rh(1)-Rh(4)-Rh(3)	64.8 (1)
Rh(4)-Rh(1)-C(1)	95.3 (7)	Rh(2)-Rh(4)-Rh(3)	60.0 (1)
P(4)-Rh(1)-C(1)	100.3 (7)	Rh(1)-Rh(4)-P(3)	152.5 (1)
Rh(2)-Rh(1)-C(5)	97.4 (7)	Rh(2)-Rh(4)-P(3)	95.0 (1)
Rh(3)-Rh(1)-C(5)	44.8 (7)	Rh(3)-Rh(4)-P(3)	95.5 (1)
Rh(4)-Rh(1)-C(5)	96.2 (7)	Rh(1)-Rh(4)-C(4)	105.8 (5)
P(4)-Rh(1)-C(5)	96.6 (7)	Rh(2)-Rh(4)-C(4)	142.8 (6)
C(1)-Rh(1)-C(5)	98.3 (10)	Rh(3)-Rh(4)-C(4)	149.0 (5)
Rh(1)-Rh(2)-Rh(3)	65.1 (1)	P(3)-Rh(4)-C(4)	100.8 (5)
Rh(1)-Rh(2)-Rh(4)	59.4 (1)	Rh(1)-Rh(4)-C(7)	66.2 (4)
Rh(3)-Rh(2)-Rh(4)	60.5 (1)	Rh(2)-Rh(4)-C(7)	48.3 (4)
Rh(1)-Rh(2)-P(2)	151.0 (1)	Rh(3)-Rh(4)-C(7)	106.3 (4)
Rh(3)-Rh(2)-P(2)	98.0 (1)	P(3)-Rh(4)-C(7)	104.7 (4)
Rh(4)-Rh(2)-P(2)	92.0 (1)	C(4)-Rh(4)-C(7)	94.9 (7)
Rh(1)-Rh(2)-C(2)	107.2 (6)	Rh(1)-Rh(4)-C(8)	83.4 (4)
Rh(3)-Rh(2)-C(2)	141.7 (5)	Rh(2)-Rh(4)-C(8)	110.9 (4)
Rh(4)-Rh(2)-C(2)	150.6 (5)	Rh(3)-Rh(4)-C(8)	51.6 (4)
P(2)-Rh(2)-C(2)	100.5 (6)	P(3)-Rh(4)-C(8)	99.5 (5)
Rh(1)-Rh(2)-C(6)	84.2 (4)	C(4)-Rh(4)-C(8)	99.4 (7)
Rh(3)-Rh(2)-C(6)	50.9 (4)	C(7)-Rh(4)-C(8)	148.9 (6)
Rh(4)-Rh(2)-C(6)	110.9 (4)	Rh(3)-P(1)-C(9)	111.6 (4)
P(2)-Rh(2)-C(6)	103.8 (4)	Rh(3)-P(1)-C(26)	116.6 (3)
C(2)-Rh(2)-C(6)	92.0 (7)	Rh(3)-P(1)-C(36)	114.0 (3)
Rh(1)-Rh(2)-C(7)	67.4 (4)	Rh(2)-P(2)-C(9)	107.5 (4)
Rh(3)-Rh(2)-C(7)	109.5 (4)	Rh(2)-P(2)-C(46)	117.8 (3)
Rh(4)-Rh(2)-C(7)	51.2 (4)	Rh(2)-P(2)-C(56)	117.0 (3)
P(2)-Rh(2)-C(7)	99.5 (4)	Rh(4)-P(3)-C(9)	106.7 (4)
C(2)-Rh(2)-C(7)	100.1 (7)	Rh(4)-P(3)-C(66)	117.5 (3)
C(6)-Rh(2)-C(7)	151.3 (6)	Rh(4)-P(3)-C(76)	119.7 (3)
Rh(1)-Rh(3)-Rh(2)	56.1 (1)	Rh(1)-P(4)-O(9)	113.9 (6)
Rh(1)-Rh(3)-Rh(4)	56.2 (1)	Rh(1)-P(4)-O(10)	120.3 (6)
Rh(2)-Rh(3)-Rh(4)	59.5 (1)	Rh(1)-P(4)-O(11)	119.2 (6)
Rh(1)-Rh(3)-P(1)	139.5 (1)	Rh(1)-C(1)-O(1)	177.1 (22)
Rh(2)-Rh(3)-P(1)	88.5 (1)	Rh(2)-C(2)-O(2)	174.9 (17)
Rh(4)-Rh(3)-P(1)	90.7 (1)	Rh(3)-C(3)-O(3)	179.0 (16)
Rh(1)-Rh(3)-C(3)	125.4 (6)	Rh(4)-C(4)-O(4)	174.0 (16)
Rh(2)-Rh(3)-C(3)	151.2 (5)	Rh(1)-C(5)-Rh(3)	98.3 (10)
Rh(4)-Rh(3)-C(3)	148.7 (5)	Rh(1)-C(5)-O(5)	132.7 (18)
P(1)-Rh(3)-C(3)	95.0 (6)	Rh(3)-C(5)-O(5)	128.3 (17)
Rh(1)-Rh(3)-C(5)	36.9 (7)	Rh(2)-C(6)-Rh(3)	81.8 (5)
Rh(2)-Rh(3)-C(5)	87.8 (7)	Rh(2)-C(6)-O(6)	143.7 (13)
Rh(4)-Rh(3)-C(5)	86.9 (6)	Rh(3)-C(6)-O(6)	134.2 (12)
P(1)-Rh(3)-C(5)	176.3 (7)	Rh(2)-C(7)-Rh(4)	80.5 (6)
C(3)-Rh(3)-C(5)	88.6 (9)	Rh(2)-C(7)-O(7)	143.4 (12)
Rh(1)-Rh(3)-C(6)	76.3 (4)	Rh(4)-C(7)-O(7)	136.1 (11)
Rh(2)-Rh(3)-C(6)	47.2 (4)	Rh(3)-C(8)-Rh(4)	83.2 (5)
Rh(4)-Rh(3)-C(6)	106.3 (4)	Rh(3)-C(8)-O(8)	132.6 (11)
P(1)-Rh(3)-C(6)	94.3 (4)	Rh(4)-C(8)-O(8)	143.2 (12)
C(3)-Rh(3)-C(6)	103.9 (6)	P(1)-C(9)-P(2)	105.8 (6)
C(5)-Rh(3)-C(6)	83.7 (7)	P(1)-C(9)-P(2)	105.9 (6)
Rh(1)-Rh(3)-C(8)	74.5 (4)	P(2)-C(9)-P(3)	107.1 (6)

Table VII. Temperature Dependence of k_1 and k_2 for CO Substitution by L on $Co_4(CO)_9[HC(PPh_2)_3]$ in DME Solvent

L	temp, °C	10^4k_1, s^{-1}	10^3k_2, M^{-1} s^{-1}
$P(OMe)_3$	41	5.09 (0.04)[a]	5.15 (0.08)
$P(n\text{-}Bu)_3$	21	0.529 (0.030)	3.61 (0.03)
	31	2.94 (0.18)	6.97 (0.14)
	36	5.26 (0.23)	10.8 (0.2)
	41	6.68 (0.28)	10.5 (0.1)
	52	41.5 (1.6)	22.7 (1.3)

[a] Values in parentheses represent one standard deviation.

The reaction between $Co_4(CO)_9[HC(PPh_2)_3]$ and $AsPh_3$ to form $Co_4(CO)_8[HC(PPh_2)_3](AsPh_3)$ does not go to completion and an equilibrium mixture of $Co_4(CO)_9[HC(PPh_2)_3]$ and $Co_4(CO)_8[HC(PPh_2)_3](AsPh_3)$ was observed with up to a 1360 molar excess of $AsPh_3$.

Table VIII. Activation Parameters for the Ligand Independent Term (k_1) for CO Substitution by L on $M_4(CO)_9[HC(PPh_2)_3]$ Clusters

M	L	$\Delta H_1^{\ddagger}$,[a] kcal/mol	$\Delta S_1^{\ddagger}$,[a] cal/(mol·K)
Co	^{13}CO[b]	24.2 ± 3.3	−0.52 ± 10.2
	$P(n\text{-}Bu)_3$[c]	25.1 ± 1.9	7.5 ± 6.2
Rh	PPh_3[c]	26 ± 2	23 ± 7
	PPh_3[d]	22.0 ± 0.4	8.9 ± 1.4

[a] Values in parentheses represent one standard deviation. [b] Reference 6b, DME solvent. [c] DME solvent. [d] CH_2Cl_2 solvent.

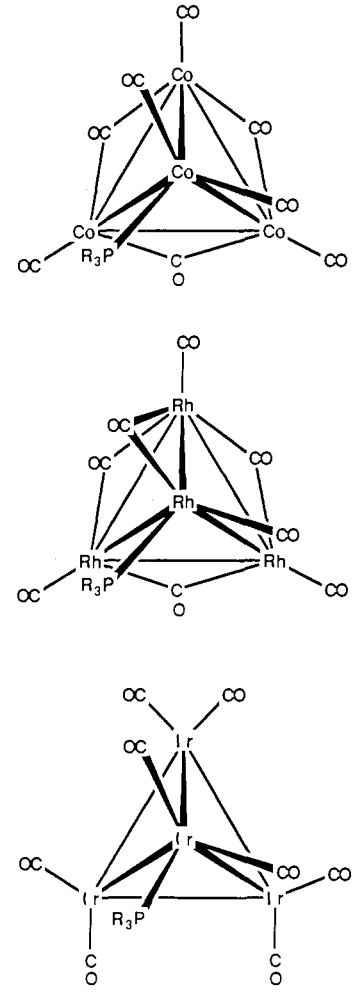

Figure 3. Structures of monosubstituted tripod carbonyl clusters of Co, Rh, and Ir. The tripod ligand capping the basal plane is not shown.

Reaction between $Rh_4(CO)_9[HC(PPh_2)_3]$ and Ligand L. The spectroscopic data in Table I and Supplementary Table II show that all $Rh_4(CO)_8[HC(PPh_2)_3]L$ clusters formed on addition of L have similar IR and ^{31}P NMR spectra. The ^{31}P NMR spectra are particularly useful for structural elucidation, and in Figure 4 we see spectra for the L = $P(OEt)_3$ and $P(O\text{-}i\text{-}Pr)_3$ derivatives. The signal for the ligand L = phosphite appears as a multiplet at δ = 100–200 ppm, slightly upfield of the signal for the free ligand. The multiplet has a splitting pattern of an overlapping doublet of quartets. One-bond phosphorus (phosphite)–rhodium couplings are about 200 Hz and three-bond phosphorus (phosphite)–phosphorus ($HC(PPh_2)_3$) couplings are about 100 Hz. The signal for the PPh_3 ligand also appears as an overlapping doublet of quartets but is shifted 100 ppm upfield of the analogous phosphite ligand and somewhat downfield of the free ligand signal. Also, with PPh_3, the coupling constants are less than those of the phosphite ligands (Table I).

The signal for the $HC(PPh_2)_3$ ligand appears as a multiplet at about 15 ppm in all clusters (Table I). The splitting pattern of the multiplet is an overlapping doublet of doublets with some

(8) Darensbourg, D. J.; Zalewski, D. J.; Rheingold, A. L.; Durney, R. L. *Inorg. Chem.* **1986**, *25*, 3281.

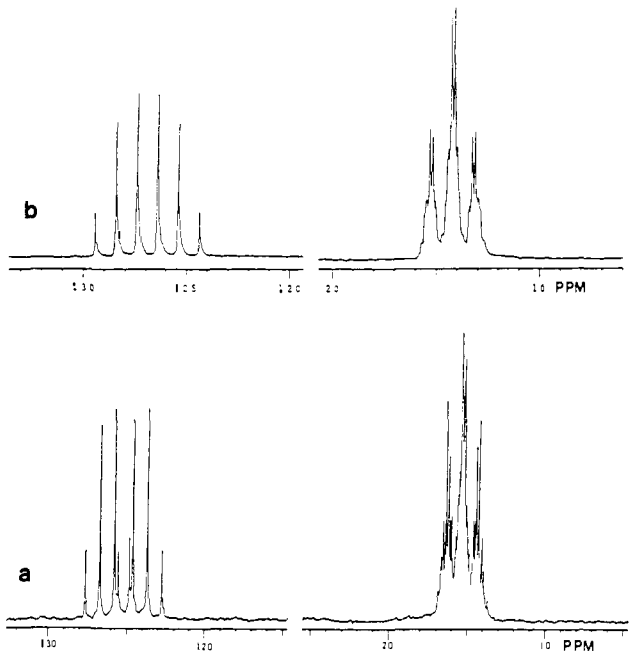

Figure 4. $^{31}P\{^1H\}$ NMR spectra of (a) $Rh_4(CO)_8[HC(PPh_2)_3][P(O\text{-}i\text{-}Pr)_3]$ and (b) $Rh_4(CO)_8[HC(PPh_2)_3][P(OEt)_3]$ at 22 °C in CD_2Cl_2.

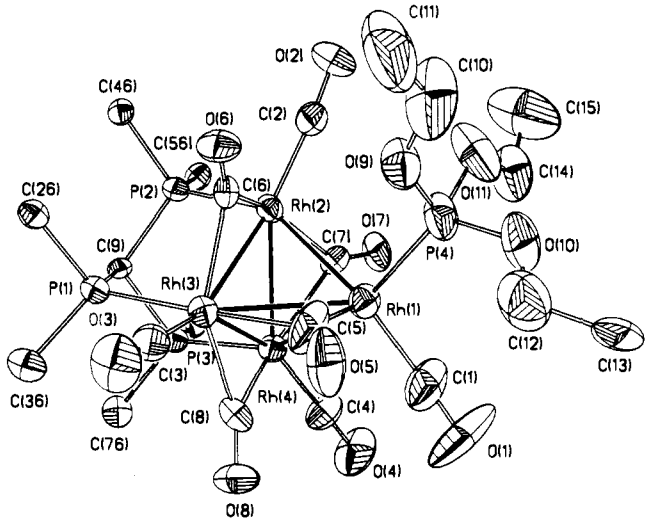

Figure 5. ORTEP plot and atom numbering scheme for $Rh_4(CO)_8[HC(PPh_2)_3][P(OEt)_3]$. Phenyl groups for the tripod ligand are not shown.

undetermined finer splittings (Figure 4). Both one-bond phosphorus $(HC(PPh_2)_3)$–rhodium couplings and 3-bond phosphorus $(HC(PPh_2)_3)$–phosphorus (phosphite) couplings are about 100 Hz.

X-ray Structure of $Rh_4(CO)_8[HC(PPh_2)_3][P(OEt)_3]$. The X-ray structure of the $P(OEt)_3$ derivative was determined (Figure 5) to definitively assign the structure of the family of monosubstituted tripod clusters of Rh. The structure resembles that of the monosubstituted cobalt tripod clusters[8] except an apical carbonyl group [C(5)O(5)] bridges between the apical Rh(1) and basal Rh(3) atoms. This bridging is highly asymmetric with Rh(1)–C(5) = 1.77 (2) Å and Rh(3)–C(5) = 2.08 (2) Å, which might be better described as a bent semibridging interaction with Rh(1)–C(5)–O(5) = 132.7 (18)°. The Rh(1)–Rh(3) bond length (Table V) significantly exceeds all other Rh–Rh bond lengths in the 60 valence electron cluster and may signal the transformation to a butterfly structure.[9] Normally μ-CO bridging does not enlongate metal–metal bonds (like a μ-H bridge does).

(9) See, for example: Bradley, J. S.; Ansell, G. B.; Hill, E. W. *J. Am. Chem. Soc.* **1979**, *101*, 7417.

Table IX. Temperature Dependence of k_1 and k_2 for CO Substitution by L on $Rh_4(CO)_9[HC(PPh_2)_3]$ in DME Solvent

L	temp, °C	10^2k_1,[a] s^{-1}	k_2, M^{-1} s^{-1}
PPh_3	22	4.91 (0.12)	
	28	9.13 (0.01)	
	41	89 (9)	
	50	204 (1)	
$P(OMe)_3$	22		$5.15\ (0.08) \times 10^{2\,a}$
	41		$8.85\ (1.45) \times 10^{2\,b}$
	50		1.21×10^3
$P(n\text{-}Bu)_3$	22		$9.5\ (1.5) \times 10^{3\,a}$
	31		$1.33\ (0.1) \times 10^{4\,b}$
	41		$1.90\ (0.06) \times 10^{4\,b}$
	50		$2.55\ (0.04) \times 10^{4\,b}$

[a] Values in parentheses represent one standard deviation on the intercept employing k_{obs} values averaged for 3–7 determinations. [b] Values in parentheses represent one standard deviation on the mean divided by [L].

Table X. Activation Parameters for the Ligand-Dependent Term (k_2) for CO Substitution by L on $M_4(CO)_9[HC(PPh_2)_3]$ Clusters

M	L	$\Delta H_2^{\ddagger}$,[a] kcal/mol	$\Delta S_2^{\ddagger}$,[a] cal/(mol·K)
Co	$P(n\text{-}Bu)_3$[b]	10.3 (1.1)	−34.4 (3.5)
Rh	$P(OMe)_3$[b]	5.1 (0.4)	−29.0 (1.2)
	$P(OMe)_3$[c]	6.7 (0.3)	−24.2 (1.0)
	$P(O\text{-}i\text{-}Pr)_3$[c]	7.6 (0.2)	−22.6 (0.8)
	$P(n\text{-}Bu)_3$[b]	6.1 (0.1)	−19.8 (0.1)
Ir	$P(OMe)_3$[b]	14.2 (2.7)	−40.6 (8.1)
	$P(n\text{-}Bu)_3$[b]	11.3 (2.7)	−45.8 (8.0)

[a] Values in parentheses represent one standard deviation. [b] DME solvent. [c] CH_2Cl_2 solvent.

Kinetics of Substitution in $Rh_4(CO)_9[HC(PPh_2)_3]$. Conventional techniques could not be employed to measure the kinetics of the CO substitution reaction (eq 3) as the rates of reaction are rapid.

$$Rh_4(CO)_9[HC(PPh_2)_3] + L \rightarrow Rh_4(CO)_8[HC(PPh_2)_3]L + CO \quad (3)$$

$$L = P(n\text{-}Bu)_3,\ P(O\text{-}i\text{-}Pr)_3,\ P(OMe)_3,\ PPh_3$$

The use of stopped-flow methods (UV–visible monitor) or a low-temperature UV–visible–IR cell enabled kinetic data to be obtained. The kinetics for the substitution of CO by L in $Rh_4(CO)_9[HC(PPh_2)_3]$ are reported for DME and CH_2Cl_2 solvents. First-order plots were linear for a least 3 half-lives from either the stopped-flow or low-temperature methods. In DME solvent, the reaction obeys a primarily ligand independent rate law for L = PPh_3 (eq 4). The kinetic data for the reaction are listed in

$$-d[Rh_4(CO)_9(HC(PPh_2)_3)]/dt = k_1[Rh_4(CO)_9(HC(PPh_2)_3)] \quad (4)$$

Table IX. At 41 °C the rate constant, k_1, is about 0.9 s^{-1}. Activation parameters determined from an Eyring plot are 26 kcal/mol ($\Delta H_1^{\ddagger}$) and 23 cal/(mol·K) ($\Delta S_1^{\ddagger}$) for the reaction of eq 3 (Tables IX and VIII).

Substitution reactions with smaller or more nucleophilic ligands (e.g. $P(OMe)_3$ or $P(n\text{-}Bu)_3$), in DME, were more rapid than with PPh_3 and obeyed a ligand-dependent rate law (eq 5). The kinetic

$$-d[Rh_4(CO)_9(HC(PPh_2)_3)]/dt = k_2[L][Rh_4(CO)_9(HC(PPh_2)_3)] \quad (5)$$

data obtained are listed in Table IX for the reaction where L = $P(OMe)_3$ and $P(n\text{-}Bu)_3$. At 41 °C the k_2 values are 885 M^{-1} s^{-1} and 1.90×10^4 M^{-1} s^{-1} for L = $P(OMe)_3$ and L = $P(n\text{-}Bu)_3$, respectively. Activation parameters calculated from the temperature dependence of k_2 in DME for L = $P(OMe)_3$ are 5.1 kcal/mol ($\Delta H_2^{\ddagger}$) and −29.0 cal/(mol·K) ($\Delta S_2^{\ddagger}$). For L = $P(n\text{-}Bu)_3$ they are 6.1 kcal/mol ($\Delta H_2^{\ddagger}$) and −19.8 cal/(mol·K) ($\Delta S_2^{\ddagger}$) (Table X).

In CH_2Cl_2 solvent, the reaction between PPh_3 and $Rh_4(CO)_9[HC(PPh_2)_3]$ (eq 3) follows a two-term rate law (eq 6).

Table XI. Temperature Dependence of k_1 and k_2 for CO Substitution by L on $Rh_4(CO)_9[HC(PPh_2)_3]$ in CH_2Cl_2 Solvent

L	pK_a[a]	θ[b]	temp, °C	10^2k_1,[c] s^{-1}	k_2, M^{-1} s^{-1}
PPh_3	2.73	145	32	8.33	3.35
			26	4.94 (0.30)	3.6 (1.7) × 10^{-1}
			19	1.70 (0.03)	4.24 (0.20) × 10^{-1}
			1.0	1.32 (0.02)	1.97 (0.10) × 10^{-2}
			−12	0.17 (0.08)	6.42 (0.30) × 10^{-3}
P(O-*i*-Pr)$_3$	4.0	130	17		112 (1)
			0.0		52.8
			−20		15.4
$P(OMe)_3$	2.60	107	17		277 (4)
			0.0		120
			−16.5		53.7
P(*n*-Bu)$_3$	8.43	132	20		8.63 (0.19) × 10^3

[a] With values collected in: Golovin, M. N.; Rahman, M. M.; Belmonte, J. E.; Giering, W. P. *Organometallics* **1985**, *4*, 1981. [b] Tolman, C. A. *Chem. Rev.* **1977**, *77*, 313. [c] Values in parentheses represent one standard deviation.

Table XI lists the kinetic data obtained for this reaction. The k_1 and k_2 values determined from the intercept and slope, respectively, of the line from k_{obs} vs $[PPh_3]$ plots are 1.70 × 10^{-2} s^{-1} and 4.24 × 10^{-1} M^{-1} s^{-1} at 19 °C. The $\Delta H_1^{\ddagger}$ and $\Delta S_1^{\ddagger}$ values, listed in Table VIII, are 22.0 kcal/mol and 8.9 cal/(mol·K), respectively, for the first-order term.

$$-d[Rh_4(CO)_9(HC(PPh_2)_3)]/dt = (k_1 + k_2[PPh_3])[Rh_4(CO)_9(HC(PPh_2)_3)] \quad (6)$$

As observed in DME solvent, the substitution of CO on $Rh_4(CO)_9[HC(PPh_2)_3]$ by smaller or more nucleophilic ligands than PPh_3 (L = $P(OMe)_3$, P(O-*i*-Pr)$_3$, P(*n*-Bu)$_3$) increases the reaction rate and switches the mechanism to a primarily ligand-dependent path. At 17 °C the k_2 values in CH_2Cl_2 for L = $P(OMe)_3$ and P(O-*i*-Pr)$_3$ are 277 M^{-1} s^{-1} and 122 M^{-1} s^{-1}, respectively. At 20 °C the k_2 value, in CH_2Cl_2, for L = P(*n*-Bu)$_3$, is about 8.6 × 10^3 M^{-1} s^{-1}. The k_1 contribution was negligible. Table XI lists the temperature dependence of the k_2 values for the reaction in eq 3 when L = $P(OMe)_3$, P(O-*i*-Pr)$_3$, and P(*n*-Bu)$_3$. From these data, activation parameters for L = $P(OMe)_3$ and P(O-*i*-Pr)$_3$ were calculated over a 35 deg temperature range and are listed in Table X. With L = $P(OMe)_3$, $\Delta H_2^{\ddagger}$ = 6.7 kcal/mol and $\Delta S_2^{\ddagger}$ = −24.2 cal/(mol·K), and with L = P(O-*i*-Pr)$_3$, $\Delta H_2^{\ddagger}$ = 7.6 kcal/mol and $\Delta S_2^{\ddagger}$ = −22.6 cal/(mol·K). None of the reactions were affected by the radical inhibitor duroquinone.

Reaction between $Ir_4(CO)_9[HC(PPh_2)_3]$ and Ligand L. The cluster $Ir_4(CO)_9[HC(PPh_2)_3]$ has previously been characterized in solution[4b,10] and in the solid state.[10] The $^{13}C\{^1H\}$ NMR spectrum of highly ^{13}CO enriched $Ir_4(CO)_9[HC(PPh_2)_3]$ at 25 °C shows an intriguing shape to the quartet signal assigned to the apical carbonyls. The splitting is not sharp and the central two peaks are much broader than the outer two peaks. This same shape is observed in the $^{31}P\{^1H\}$ NMR spectrum of highly ^{13}CO enriched $Ir_4(CO)_9[HC(PPh_2)_3]$ at 25 °C. The shape of these signals is independent of the magnetic field (270 or 400 MHz). At higher temperatures the signal becomes a sharp quartet. We are uncertain whether these observations are indicative of an intramolecular exchange process or of second-order effects in the NMR experiment.

The clusters $Ir_4(CO)_8[HC(PPh_2)_3]L$ (L = $P(OMe)_3$, P(*n*-Bu)$_3$) were identified by comparison of the IR carbonyl stretching frequencies for these clusters with the reported[7] values for L = PPh_3 and $PPh_2C_2H_4Si(OEt)_3$ (Supplementary Table VI). The $^{31}P\{^1H\}$ NMR chemical shifts of the latter two clusters were also reported and we examined the $^{31}P\{^1H\}$ NMR spectrum of a ^{13}CO-enriched $Ir_4(CO)_8[HC(PPh_2)_3][PMe_3]$ cluster. Both the basal carbonyl and apical carbonyl signals shift downfield from the respective signals on $Ir_4(CO)_9[HC(PPh_2)_3]$. The signal of the basal carbonyl is a broad singlet at δ 170.2 and the signal of the apical carbonyl is a multiplet centered at δ 164.0. Three-bond carbon (apical)–phosphorus ($HC(PPh_2)_3$) coupling is observed (15.3 Hz) and two-bond carbon (apical)–phosphorus (PMe_3) or three-bond carbon (apical)–carbon (basal) coupling is 5.1 Hz.

(10) Clucas, J. A.; Harding, M. M.; Nicholls, B. S.; Smith, A. K. *J. Chem. Soc., Chem. Commun.* **1984**, 319.

Table XII. Temperature Dependence of k_1 and k_2 for CO Substitution by L on $Ir_4(CO)_9[HC(PPh_2)_3]$ in DME Solvent

L	temp, °C	k_1,[a] s^{-1}	k_2,[a] M^{-1} s^{-1}
^{13}CO	76	6.76 × 10^{-7}	
$P(OMe)_3$	41		1.42 × 10^{-6}
	52		2.15 (0.02) × 10^{-6}
	75		1.34 × 10^{-5}
$\Delta H_2^{\ddagger}$ = 14.2 (2.5) kcal/mol, $\Delta S_2^{\ddagger}$ = −40.6 (7.9) cal/(mol·K)			
P(*n*-Bu)$_3$	41		1.01 × 10^{-5}
	66		2.96 (0.55) × 10^{-5}
	75		7.30 (0.51) × 10^{-5}
$\Delta H_2^{\ddagger}$ = 11.2 (2.8) kcal/mol, $\Delta S_2^{\ddagger}$ = −46.1 (8.5) cal/(mol·K)			

[a] Values in parentheses represent one standard deviation.

Kinetic data have been obtained for the exchange reaction of ^{13}CO and $Ir_4(CO)_9[HC(PPh_2)_3]$ at 79 °C in DME solvent. The composite spectra of the exchange reaction (eq 7) (L = ^{13}CO) for the first two half-lives of reaction exhibit a first-order dependence on $Ir_4(CO)_9[HC(PPh_2)_3]$ concentration. Carbonyl

$$Ir_4(CO)_9[HC(PPh_2)_3] + L \rightarrow Ir_4(CO)_8[HC(PPh_2)_3]L + CO \quad (7)$$

$$L = {}^{13}CO,\ P(OMe)_3,\ P(n\text{-}Bu)_3$$

exchange reactions typically obey ligand-independent rate laws for neutral, low-valent metal carbonyl compounds and we infer that the reaction, with L = ^{13}CO, obeys a ligand-independent rate law (eq 8). Therefore at 76 °C, in DME solvent, k_1 is about 6.8

$$-d[Ir_4(CO)_9(HC(PPh_2)_3)]/dt = k_1[Ir_4(CO)_9(HC(PPh_2)_3)] \quad (8)$$

× 10^{-7} s^{-1} for CO dissociation from $Ir_4(CO)_9[HC(PPh_2)_3]$ (Table XII).

Carbonyl substitution by $P(OMe)_3$ or P(*n*-Bu)$_3$ in $Ir_4(CO)_9[HC(PPh_2)_3]$ (eq 7) in DME proceeds cleanly as evidenced by the presence of isosbestic points in the composite carbonyl stretching region IR spectra. The substitution reactions follow a predominantly ligand dependent rate law (eq 9). Plots of k_{obs} vs ligand concentration yield k_1 values equal to 0, within experimental error. The ligand-dependent rate constants, k_2, at 75 °C in DME solvent are 1.34 × 10^{-5} M^{-1} s^{-1} and 7.30 × 10^{-5} M^{-1} s^{-1} for L = $P(OMe)_3$ and P(*n*-Bu)$_3$, respectively (Table XII). The activation parameters derived from the data are 14.2 kcal/mol ($\Delta H_2^{\ddagger}$) and −40.6 cal/(mol·K) ($\Delta S_2^{\ddagger}$) when L = $P(OMe)_3$ and 11.2 kcal/mol ($\Delta H_2^{\ddagger}$) and −46.1 cal/(mol·K) ($\Delta S_2^{\ddagger}$) when L = P(*n*-Bu)$_3$ (Table XII).

$$-d[Ir_4(CO)_9(HC(PPh_2)_3)]/dt = k_2[L][Ir_4(CO)_9(HC(PPh_2)_3)] \quad (9)$$

$$L = P(OMe)_3,\ P(n\text{-}Bu)_3$$

Selective enrichment of ^{13}CO into the apical position of $Ir_4(CO)_9[HC(PPh_2)_3]$ has been reported.[4b] We found that a statistical distribution of ^{13}CO about the cluster framework could be observed under low ^{13}CO pressures (≤2 atm) at temperatures above 75 °C and extended reaction times (weeks). Only at shorter reaction times could selective enrichment be achieved. These observations suggest that apical to basal intramolecular carbonyl exchange occurs slowly. A sample of $Ir_4(CO)_9[HC(PPh_2)_3]$, selectively enriched with ^{13}CO in the apical position, was allowed to react with PMe_3 at ambient temperature in CD_2Cl_2. The resulting ^{13}C NMR spectrum shows a migration of ^{13}CO into the basal sites on formation of $Ir_4(CO)_9[HC(PPh_2)_3](PMe_3)$. The $^{13}C\{^1H\}$ NMR spectra for this experiment are shown in Figure 6.

Reaction between $Rh_4(CO)_8[HC(PPh_2)_3]L$ and Ligand L. No observable reaction occurs between $Rh_4(CO)_8[HC(PPh_2)_3](PPh_3)$ and excess PPh_3 at 25 °C over a several hour period. In contrast,

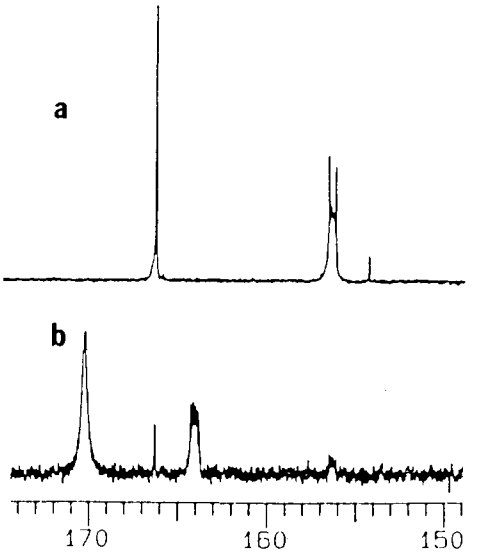

Figure 6. $^{13}C\{^1H\}$ NMR spectra of the reaction between $Ir_4(CO)_9[HC(PPh_2)_3]$, selectively enriched in the apical position, and PMe_3 in CD_2Cl_2 at 20 °C: (a) $Ir_4(CO)_9[HC(PPh_2)_3]$; (b) $Ir_4(CO)_8[HC(PPh_2)_3](PMe_3)$.

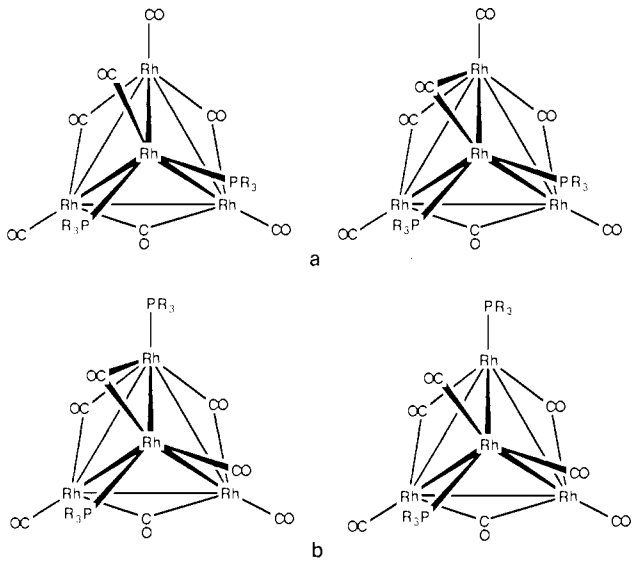

Figure 7. Illustration of the structures of (a) $Rh_4(CO)_7[HC(PPh_2)_3]L_2$, two possible apical-apical isomers, and (b) $Rh_4(CO)_7[HC(PPh_2)_3]L_2$, two possible apical-basal isomers. The tripod ligand is not shown.

when L = $P(OMe)_3$, $P(OEt)_3$, $P(O\text{-}i\text{-}Pr)_3$, $P(OMe)_2Ph$, or $P(n\text{-}Bu)_3$ the reaction (eq 10) proceeds rapidly at 25 °C. Identification

$$Rh_4(CO)_8[HC(PPh_2)_3]L + L \rightarrow Rh_4(CO)_7[HC(PPh_2)_3]L_2 + CO \quad (10)$$

of the products of reaction by $^{31}P\{^1H\}$ NMR spectroscopy showed that the ligands L bind in one of two arrangements. One isomer binds both ligands to the apical position; however, we do not know whether the apical CO bridges (Figure 7). In this isomer the two ligands L are equivalent at 20 °C and the $^{31}P\{^1H\}$ NMR signal multiplicity looks like that for the monosubstituted derivatives, but it is shifted downfield. This can be seen in the $^{31}P\{^1H\}$ NMR spectrum of $Rh_4(CO)_7[HC(PPh_2)_3][P(OMe)_2Ph]_2$ compared to $Rh_4(CO)_8[HC(PPh_2)_3][P(OMe)_2Ph]$ in Figure 8. For both clusters the splitting pattern is an overlapping doublet of quartets. The chemical shift of the disubstituted product is at about 156.5 ppm, downfield from the monosubstituted signal at about 151 ppm. The $^{31}P\{^1H\}$ NMR data for several derivatives of this isomer of $Rh_4(CO)_7[HC(PPh_2)_3]L_2$ are listed in Table II.

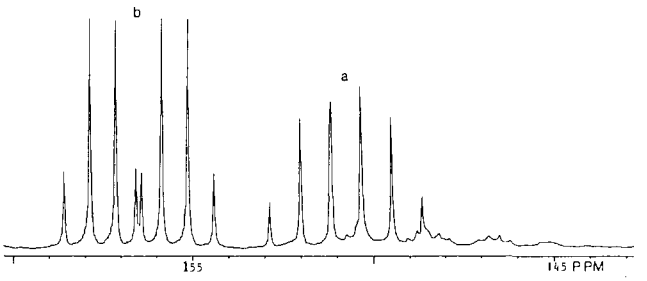

Figure 8. $^{31}P\{^1H\}$ NMR spectra of a CD_2Cl_2 solution at 22 °C: (a) $Rh_4(CO)_8[HC(PPh_2)_3][P(OMe)_2Ph]$ and (b) $Rh_4(CO)_7[HC(PPh_2)_3][P(OMe)_2Ph]_2$, apical-apical isomer.

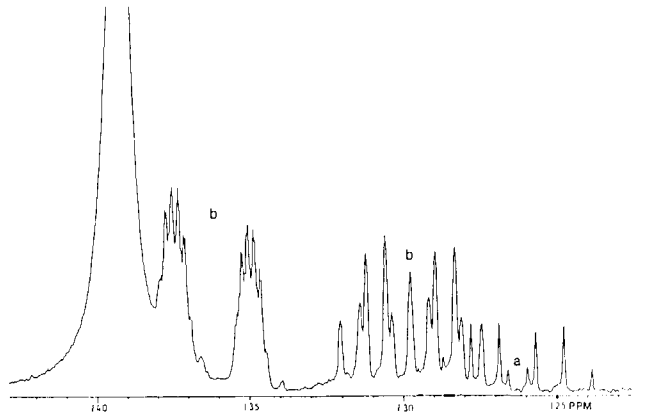

Figure 9. $^{31}P\{^1H\}$ NMR spectra of a CD_2Cl_2 solution at 22 °C: (a) $Rh_4(CO)_7[HC(PPh_2)_3][P(O\text{-}i\text{-}Pr)_3]_2$, apical-apical isomer, and (b) $Rh_4(CO)_7[HC(PPh_2)_3][P(O\text{-}i\text{-}Pr)_3]_2$, apical-basal isomer.

The other substitution product observed from the reaction (eq 10) has one apical bonded L and one basal-radial bonded L. For this product there are several additional isomers possible depending on the carbonyl configuration, one of which is shown in Figure 7. The structures of these clusters are outlined in Figure 7. We have not been able to distinguish which isomer is present in solution. Figure 9 shows the $^{31}P\{^1H\}$ NMR spectrum for the $P(O\text{-}i\text{-}Pr)_3$ signals of a solution containing both the apical-apical and apical-basal bonded isomers of $Rh_4(CO)_7[HC(PPh_2)_3][P(O\text{-}i\text{-}Pr)_3]_2$. Whereas the apical-apical isomer exhibits an overlapping doublet of quartets splitting pattern, the apical-bonded $P(O\text{-}i\text{-}Pr)_3$ ligand of the apical-basal isomer shows a symmetric eleven-line signal with a relative intensity pattern of 1:1:2:2:1:2:1:2:2:1:1. This is interpreted as an overlapping double triplet of doublets. This signal appears downfield from the apical-apical isomer. Further downfield, but slightly upfield from the free ligand signal, is the basal-bonded $P(O\text{-}i\text{-}Pr)_3$ signal, and this shows up as a doublet of multiplets. The $^{31}P\{^1H\}$ NMR data for observed derivatives of this isomer are listed in Table II. The signal for the $HC(PPh_2)_3$ ligand typically shows up as an overlapping doublet of triplets for the apical-apical isomer and as two signals, both multiplets, for the apical-basal isomer. The observation that the ligands L are equivalent in the apical-apical isomer indicates a low-energy intramolecular exchange path about the axial center.

Generally, both isomers are found in solution although the apical-apical isomer forms first. Efforts to separate the two isomers proved fruitless in our hands. Fractional crystallization or column chromatography over silica gel or alumina did not succeed, although samples enriched in one isomer over the other were obtainable. In Supplementary Table V are reported the carbonyl stretching frequencies of several derivatives.

Several kinetic experiments were conducted on reactions outlined in eq 10 to determine the rate of formation of the apical-apical substituted isomer, since this was the first product observed in the NMR experiments. As noted, formation of the apical-basal isomer began before complete formation of the apical-apical isomer. The IR spectra of samples containing mostly the api-

Table XIII. Temperature Dependence of k_1 and k_2 for CO Substitution by $P(OEt)_3$ on $Rh_4(CO)_8[HC(PPh_2)_3][P(OEt)_3]$ in CH_2Cl_2[a]

temp, °C	k_1, s^{-1}	k_2, M^{-1} s^{-1}
22	6.9 (2.3) × 10^{-4}	1.17 (0.03) × 10^{-1}
10		5.5 × 10^{-2}
0		2.8 × 10^{-2}
−10		1.3 × 10^{-2}

[a] $\Delta H_2^{\ddagger}$ = 10.0 (0.1) kcal/mol. $\Delta S_2^{\ddagger}$ = −28.8 (0.1) cal/(mol·K).

cal-apical isomer had carbonyl stretching bands overlapping those of the monosubstituted reactant cluster. Because pure solutions of the apical-apical isomer were not obtained, kinetic data were more difficult to determine. In the case of L = $P(O\text{-}i\text{-}Pr)_3$ and $P(n\text{-}Bu)_3$, nonlinear pseudo-first-order plots of ln A vs time were observed. For the reactions with L = $P(OEt)_3$, isosbestic points were observed initially and these data were of adequate quality to determine the reported rates. For the reaction between $Rh_4(CO)_8[HC(PPh_2)_3][P(OEt)_3]$ and $P(OEt)_3$ a plot of the initial k_{obs} vs $P(OEt)_3$ concentration showed the reaction obeys a two-term rate law (eq 11); however, the ligand-independent term

$$-d[Rh_4(CO)_8(HC(PPh_2)_3)(P(OEt)_3)]/dt = (k_1 + k_2[P(OEt)_3])[Rh_4(CO)_8(HC(PPh_2)_3)(P(OEt)_3)] \quad (11)$$

contributes less than 30% to the overall rate under the reaction conditions. Because the k_1 term should contribute even less at lower temperatures the k_2 values at these temperatures were determined from eq 12. These data are given in Table XIII along

$$k_2 = k_{obs}/[P(OEt)_3] \quad (12)$$

with the activation parameters calculated from the Eyring plot for the k_2 term. The enthalpy of activation ($\Delta H_2^{\ddagger}$) was found to be about 10 kcal/mol and the entropy of activation ($\Delta S_2^{\ddagger}$) to be about −29 cal/(mol·K), consistent with an associative process.

Discussion

Structures of Substitution Products $M_4(CO)_8[HC(PPh_2)_3]L$. Various $Co_4(CO)_8[HC(PPh_2)_3]L$ clusters have been prepared[4a,6a,8,11] and found to be substituted at the apical metal center as confirmed crystallographically for $Co(CO)_8[HC(PPh_2)_3](PMe_3)$.[8] IR spectra of the new derivatives of $Co_4(CO)_8[HC(PPh_2)_3]L$ (L = $P(OMe)_3$, $P(n\text{-}Bu)_3$) examined in this study resemble those reported previously (Supplementary Table I) and are thus assigned the same structure.

All the IR spectra for $Rh_4(CO)_8[HC(PPh_2)_3]L$ clusters are similar and suggest a common structure (Supplementary Table II). The assignment of the apical position as the site of L bonding is most clearly seen in the $^{31}P\{^1H\}$ NMR spectra of $Rh_4(CO)_8[HC(PPh_2)_3]L$ (Table I). One signal is observed for the tripod ligand, implying equivalence of the three phosphorus centers. The signal for the ligand L shows up as a multiplet in the general region of the free ligand chemical shift. In some cases the multiplet is eight lined with relative intensities of 1:3:3:1:1:3:3:1 and is clearly an overlapping doublet of quartets (e.g., L = $P(O\text{-}i\text{-}Pr)_3$; Figure 6). On the basis of an apical substituted structure the doublet arises from one-bond phosphorus coupling to the apical rhodium center and the quartet from three-bond phosphorus–phosphorus coupling between the phosphite (or phosphine) and the three equivalent phosphorus centers of the tripod ligand. In other cases the multiplet is six lined with relative intensities of 1:3:4:4:3:1 (e.g., L = $P(OEt)_3$). In terms of an apical substituted species, the multiplet is interpreted as an overlapping doublet of quartets in which there is coincidence of two pairs of lines from each quartet.

The signal for the tripod ligand appears as a multiplet and generally looks like a triplet with finer splittings (Figure 6). The apparent triplet is instead an overlapping doublet (from coupling to the directly bound rhodium center) of doublets (from three-bond phosphorus–phosphorus coupling between the equivalent phosphorus centers of the tripod ligand and the apical bond ligand L). The coupling constant of the latter doublet should equal that measured from the apical ligand if the assignments of structure and couplings are correct. This was confirmed in all cases. The observation of equivalence of the three phosphorus centers of the $HC(PPh_2)_3$ ligand implies a rapid localized exchange of carbonyl and phosphorus ligands about the apical rhodium center at room temperature. Carbonyl exchange about the apical center was also rapid[4b] in $Rh_4(CO)_8[HC(PPh_2)_3]L$. Given the solid-state structure of $Rh_4(CO)_8[HC(PPh_2)_3][P(OEt)_3]$, which shows a semibridging CO between the apical Rh and a basal Rh, it is possible that a similar structure persists in solution. Rapid exchange of the two apical CO's seems likely and would account for the simplified NMR spectra.

The $Ir_4(CO)_8[HC(PPh_2)_3]L$ clusters have not been as fully characterized as the rhodium clusters. The carbonyl stretching frequencies for L = $P(OMe)_3$ and $P(n\text{-}Bu)_3$ are similar to those reported[7] for L = PPh_3 and $PPh_2C_2H_4Si(OEt)_3$ (Supplementary Table IV). In all cases no absorptions were observed in the bridging carbonyl region of the IR spectra. One signal each was reported[7] in the $^{31}P\{^1H\}$ NMR spectra of $Ir_4(CO)_8[HC(PPh_2)_3]L$ (L = PPh_3, $PPh_2C_2H_4Si(OEt)_3$), indicating equivalence of the phosphorus centers of the tripod ligand. Additionally, the $^{13}C\{^1H\}$ NMR spectrum of $Ir_4(CO)_8[HC(PPh_2)_3](PMe_3)$ exhibits no resonance in the bridging carbonyl region and one signal each for the apical carbonyls and basal carbonyls in the terminal carbonyl region. Both the apical and basal carbonyl ^{13}C NMR chemical shifts in $Ir_4(CO)_8[HC(PPh_2)_3](PMe_3)$ are downfield from $Ir_4(CO)_9[HC(PPh_2)_3]$. Therefore, the spectroscopic data strongly suggest simple substitution of an apical terminal CO by L.

Mechanism of CO Substitution in $M_4(CO)_9[HC(PPh_2)_3]$. The kinetics of the CO exchange reaction for $Co_4(CO)_9[HC(PPh_2)_3]$ (eq 1, L = ^{13}CO), in DME solvent, have been previously reported.[6b] The reported k_1 values were suggested to represent the CO dissociative rate constants and a statistical correction was applied to the observed rate constants based on the spectroscopic feature used to obtain the data and the idea that one of the three apical carbonyls dissociate from the cluster. We suggest the k_1 values obtained in our reactions also represent a CO dissociative path but report them without statistical correction. Our value for $Co_4(CO)_9[HC(PPh_2)_3]$ at 52 °C (Table VII) compares well with the previous report of 1.71 × 10^{-4} s^{-1} at 40 °C, when treated the same way (i.e. our uncorrected k_1 is about three times larger than the previous report). A comparison of activation parameters for the k_1 path from the ^{13}CO exchange data and phosphine substitution data also shows good agreement within the precision of the available data. Using our data and that of Darensbourg[6] the entering ligands can be arranged qualitatively in order of increasing associative reactivity as CO < PPh_3 ~ $AsPh_3$ ≪ $P(OMe)_3$ < PMe_2Ph ~ $P(n\text{-}Bu)_3$ ≪ PMe_3. Small nucleophilic ligands (PMe_3) react much faster than bulky weak nucleophiles (PPh_3, $AsPh_3$). Between these extremes both ligand basicity and size appear to be important factors.

For $Rh_4(CO)_9[HC(PPh_2)_3]$ we were able to determine both unimolecular and bimolecular paths for CO replacement (Tables IX and XI). The activation parameters (Tables VIII and X) are consistent with k_1 belonging to a dissociative (high $\Delta H_1^{\ddagger}$, positive $\Delta S_1^{\ddagger}$) and k_2 belonging to an associative (low $\Delta H_2^{\ddagger}$, negative $\Delta S_2^{\ddagger}$) mechanism. Also, the entering ligand dependence (Table XI), with the bulky poor PPh_3 nucleophile reacting primarily by a dissociative route and the small good nucleophile $P(n\text{-}Bu)_3$ reacting by an associative path, agrees with the proposed mechanism for the k_1 and k_2 rates. Steric effects appear to dominate since $P(OMe)_3$ and $P(O\text{-}i\text{-}Pr)_3$, which are less nucleophilic but much less hindered than PPh_3, react nearly as fast as $P(n\text{-}Bu)_3$. A slight solvent effect was observed (Tables IX and XI). For PPh_3 an associative contribution to the rate law was detected in CH_2Cl_2 solvent but not in DME solvent. The rates in DME also are 2.5–3.2 faster than in CH_2Cl_2. These differences are not sig-

(11) Rimmelin, D.; Lemoine, P.; Gross, M.; Bahsoun, A. A.; Osborn, J. A. *Nouv. J. Chim.* **1985**, *9*, 181.

Scheme I

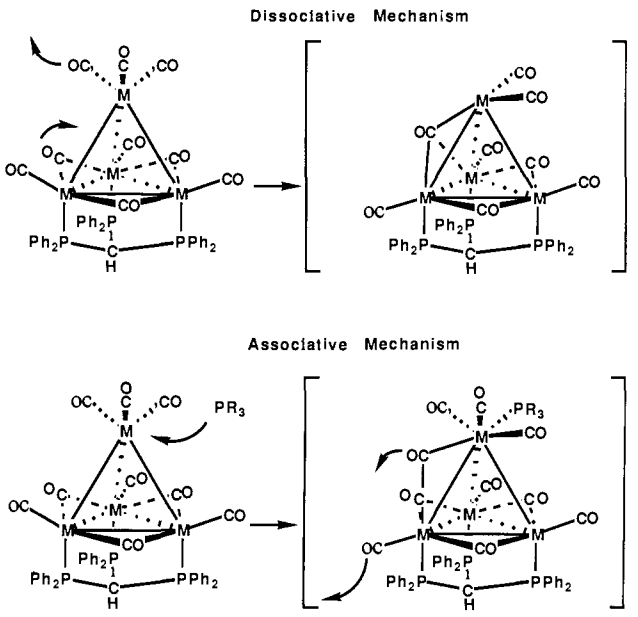

nificant enough to discuss further.

For $Ir_4(CO)_9[HC(PPh_2)_3]$ a unimolecular k_1 path was not observed for any of the phosphorus donor ligands examined. Therefore, the exchange reaction with ^{13}CO was used to estimate the rate k_1 with the assumption that it proceeds (as for most metal carbonyls) by a dissociative mechanism. The ligand dependence and activation parameters for the k_2 path qualitatively resemble those for the rhodium analogue, except the rates are greatly diminished. Dahlinger, Falcone, and Poë[12] have shown a clear relationship between entering ligand nucleophilicity and size for associative substitution in $Ir_4(CO)_{12}$.

We confirmed a previous report[4b] that ^{13}CO can be selectively incorporated into the apical position of $Ir_4(CO)_9[HC(PPh_2)_3]$. The lack of fluxionality suggests that associative reactions of this cluster, which proceed at ambient temperature, do not involve CO bridging in a rapid reversible preequilibrium before substitution occurs. The observation of ^{13}CO migration to the basal plane concomitant with CO substitution by PMe_3 (Figure 6) can arise from a mechanistic path where an apical CO bridges to the basal plane as PMe_3 attacks the apical atom (Scheme I). Alternatively, basal-apical CO exchange in the substituted product might be more rapid. Since apical substitution in $Rh_4(CO)_8[HC(PPh_2)_3][P(OEt)_3]$ promotes apical-basal CO bridging as seen in the X-ray structure (Figure 5), the latter possibility cannot be dismissed.

From the structures of the monosubstituted products, all apical substituted $M_4(CO)_8[HC(PPh_2)_3]L$, we conclude that CO dissociation and nucleophilic attack at the apical position is preferred (Scheme I). This has been proved for ^{13}CO substitution in $Co_4(CO)_8[HC(PPh_2)_3][PMe_3]$ and $Ir_4(CO)_9[HC(PPh_2)_3]$, where ^{13}CO selectively incorporates into the apical position. Furthermore, our experiments described for the addition of $P(OEt)_3$ to $Rh_4(CO)_8[HC(PPh_2)_3][P(OEt)_3]$ show the apical-apical substituted cluster forms first and slowly rearranges to a more stable apical-basal substituted species. That the apical metal would be most labile to CO dissociation and nucleophilic attack seems reasonable. In mononuclear metal carbonyls substitution of CO by PR_3 ligands generally decreases the lability of CO in both dissociative and associative mechanisms.[13] Since PR_3 ligands are better donors than CO they increase electron density on the metal atom, which increases M → CO back-bonding and decreases the electrophilicity at the metal center. Thus, decreased reactivity of the tripod substituted basal metal atoms is expected. In $Rh_4(CO)_8[HC(PPh_2)_3][P(OEt)_3]$ the apical Rh, substituted with the π-acceptor $P(OEt)_3$ ligand, should also be the favored site for nucleophilic attack over the basal sites substituted with the more basic and sterically hindered tripod ligand. The speculative mechanism depicted in Scheme I incorporates the basic tenant of apical substitution along with the suggestion that CO bridging may help relieve the electronic imbalance that occurs in the putative transition states.

Table XIV. Comparison of the k_1 (76 °C) and k_2 (41 °C) Terms for CO-Substitution Reactions of $M_4(CO)_9[HC(PPh_2)_3]$ Clusters in DME Solvent (M = Co, Rh, Ir)

cluster[a]	k_1, s^{-1}	rel k_1
$Co_4(CO)_9[HC(PPh_2)_3]$	6×10^{-2} [b]	1
$Rh_4(CO)_9[HC(PPh_2)_3]$	4×10^{1} [c]	667
$Ir_4(CO)_9[HC(PPh_2)_3]$	6.76×10^{-7}	1×10^{-5}

	L = $P(OMe)_3$		L = $P(n\text{-}Bu)_3$	
cluster[d]	k_2, M^{-1} s^{-1}	rel k_2	k_2, M^{-1} s^{-1}	rel k_2
$Co_4(CO)_9[HC(PPh_2)_3]$	5.15×10^{-3}	1	1.05×10^{-2}	1
$Rh_4(CO)_9[HC(PPh_2)_3]$	885	1.7×10^{5}	1.90×10^{4}	1.8×10^{6}
$Ir_4(CO)_9[HC(PPh_2)_3]$	1.42×10^{-6}	2.8×10^{-4}	1.01×10^{-5}	1×10^{-3}

[a] At 76 °C. [b] Estimated at 76 °C from ΔH_1^* and ΔS_1^* for L = $P(n\text{-}Bu)_3$. [c] Estimated at 76 °C from ΔH_1^* and ΔS_1^* for L = PPh_3. [d] At 41 °C.

Periodic Effects on Reactivity of the Tetrametal Core. The k_1 values for CO substitution on $M_4(CO)_9[HC(PPh_2)_3]$ (M = Co, Rh, Ir) can be compared. Since the value for M = Ir was determined by ^{13}CO exchange at 76 °C, the comparison will be made at that temperature. Values for Co and Rh will be estimated at 76 °C from the activation parameters for the reactions with $P(n\text{-}Bu)_3$ and PPh_3, respectively, in DME solvent. These values and the corresponding relative k_1 values are listed in Table XIV and indicate Rh > Co ≫ Ir for the rates of CO dissociation. At 76 °C, the CO dissociative rate constant for rhodium is about 650 times that for cobalt and about 6×10^7 times that for iridium. For all reactions measured, the enthalpy of the activation is large (>20 kcal/mol) and the entropy of activation is positive, consistent with a common dissociative process.

In a similar way, the ligand-dependent, k_2, terms can be compared. The activation parameters for the k_2 term in CO substitution reactions by ligand L on $M_4(CO)_9[HC(PPh_2)_3]$ all show typical values (Table X) for a predominantly associative process. Thus ΔH_2^* values are low (<15 kcal/mol) and ΔS_2^* values are negative. The rhodium ΔH_2^* values are less positive and ΔS_2^* values are less negative than either cobalt or iridium, indicative of a more favorable transition state for nucleophilic attack at rhodium. The k_2 values in Table XIV show a metal effect on reactivity of Rh ≫ Co > Ir. Although this parallels changes found for the k_1 rates, the difference between Rh and the other cluster species is more dramatic. Rates of nucleophilic attack at $Rh_4(CO)_9[HC(PPh_2)_3]$ exceed those at $Co_4(CO)_9[HC(PPh_2)_3]$ and $Ir_4(CO)_9[HC(PPh_2)_3]$ by 10^5–10^9.

The variation in rates of reaction as degree of ligand substitution increases can be compared for the tetranuclear carbonyl clusters of cobalt, rhodium, and iridium. For $Ir_4(CO)_9(PPh_3)_3$ a study of ^{13}CO exchange in C_2Cl_4 solvent at 80 °C[14a] compared to our value for $Ir_4(CO)_9[HC(PPh_2)_3]$ (^{13}CO exchange in DME solvent at 76 °C) yields a k_1 23 000 times larger with $Ir_4(CO)_9(PPh_3)_3$ than with $Ir_4(CO)_9[HC(PPh_2)_3]$! The solid-state structures of $Ir_4(CO)_9(PPh_3)_3$[14b] and $Ir_4(CO)_9[HC(PPh_2)_3]$[10] differ. In the former the phosphine ligand disposition in the basal region is

(12) (a) Dahlinger, K.; Falcone, F.; Poë, A. J. *Inorg. Chem.* **1986**, *25*, 2654. (b) Poë, A. J. In *Metal Clusters*; Moskovits, M., Ed.; Wiley-Interscience: New York; Chapter 4, 1986. (c) Poë, A. J. *Int. J. Chem. Kinet.* **1988**, *20*, 467. (d) Poë, A. J. *Pure Appl. Chem.* **1988**, *60*, 1209.

(13) (a) Basolo, F.; Pearson, R. G. *Mechanisms of Inorganic Reactions*, 2d ed.; John Wiley & Sons: New York, 1967. (b) Atwood, J. D. *Inorganic and Organometallic Reaction Mechanisms*; Brooks Cole Publishing Co.: Monterey, CA, 1985.

(14) (a) Darensbourg, D. J.; Baldwin-Zuschke, B. J. *J. Am. Chem. Soc.* **1982**, *104*, 3906. (b) Albano, V.; Bellow, P. L.; Scatturin, V. *Chem. Commun.* **1967**, 730.

Table XV. Physical Properties of Tetranuclear Clusters of Cobalt, Rhodium, and Iridium

compd	λ,[a] nm	E_{pc},[a] V	$\int\rho$,[a] e	ν(CO),[b] cm^{-1}	M–C^{ap}, Å	M^{ba}–M^{ap}, Å
$Co_4(CO)_9[HC(PPh_2)_3]$	760	−0.78	2.41	2050	1.793[c]	2.540[c]
$Rh_4(CO)_9[HC(PPh_2)_3]$	500	−1.14		2060		
$Ir_4(CO)_9[HC(PPh_2)_3]$	342	−1.82		2042	1.79[d]	2.684[d]
$Co_4(CO)_{12}$	660	−0.12	3.11	2103	1.834[e]	2.492[e]
$Rh_4(CO)_{12}$	303	−0.80	5.39	2101	1.99[f]	2.732[f]
$Ir_4(CO)_{12}$	321		5.40	2071	1.87[g]	2.693[g]

[a] Longest wavelength absorption, λ, cathodic peak current for the first reduction, E_{pc}, and the charge calculated for the cluster core, $\int\rho$, are from ref 5. [b] Highest frequency carbonyl stretch. [c] Reference 6b. [d] Reference 10. [e] Carre, F. H.; Cotton, F. A.; Frenz, B. A. *Inorg. Chem.* **1976**, *15*, 380. [f] Wei, C. H. *Inorg. Chem.* **1968**, *8*, 2384. [g] Churchill, M. R.; Hutchinson, J. P. *Inorg. Chem.* **1978**, *17*, 3528.

axial-diradial and three carbonyl ligands edge bridge the basal iridium atoms. The $Ir_4(CO)_9[HC(PPh_2)_3]$ cluster bonds the $HC(PPh_2)_3$ ligand in axial positions on its basal face and adopts a carbonyl ligand configuration like $Ir_4(CO)_{12}$ (i.e., no bridging carbonyls). The rate of CO dissociation in $Ir_4(CO)_9[HC(PPh_2)_3]$ resembles that in $Ir_4(CO)_{12}$. The similarity between the rates in these latter two isostructural compounds makes sense since in each case dissociation occurs from a common apical $Ir(CO)_3$ fragment. If one of the apical carbonyls dissociates selectively from $Ir_4(CO)_9[HC(PPh_2)_3]$, then a statistical correction of 1/3 can be applied to the observed k_1 value to yield a corrected k_1 value. The k_1 value for $Ir_4(CO)_9[HC(PPh_2)_3]$ is then 2.3×10^{-7} s^{-1} or about one-sixth that of $Ir_4(CO)_{12}$. This agrees with the notion that CO dissociation occurs from the apical position in $Ir_4(CO)_9[HC(PPh_2)_3]$, decreased slightly because of an increase in electron density communicated by the remote tripod substituted iridium atoms. Apparently the basal-apical tripod ligand has only a small influence on the Ir–C bond strength to the apical CO's. The unexpected enhanced reactivity in $Ir_4(CO)_9(PPh_3)_3$ may result from an effect on the bridging CO's. Indeed, $Ir_4(CO)_{12}$ is unusual in that phosphine substitution enhances the rate of CO dissociation. This was originally attributed[15] to the presence of bridging CO groups. Our data for the nonbridged tripod complex support this view and suggest that a $\sim 10^4$ difference in reactivity results from the introduction of bridging CO groups. In Scheme I we propose that this effect arises from the ease with which an edge bridging CO group becomes face bridging through a least motion path to stabilize the electron deficient apical metal atom in the dissociative intermediate. If one corrects the data in Table XIV to account for the absence of bridging CO's in $Ir_4(CO)_9[HC(PPh_2)_3]$ vs the Co and Rh analogues then the rates for Co and Ir would be comparable; however, the rhodium species still exhibits an enhanced reactivity.

Alternative explanations for the above behavior could be proposed. One would be that the tripod ligand has a higher basicity than PPh_3 and the enhanced back-bonding to the terminal CO groups decreases the dissociation rate. The basicity difference, however, cannot explain the magnitude of the effect since the rate of CO loss from $Ir_4(CO)_9[P(n\text{-}Bu)_3]_3$ and $Ir_4(CO)_4[P(i\text{-}Pr)_3]_3$ is 0.15 and 0.87 times that in the PPh_3-substituted cluster.[12] Another difference is that the tripod substitutes axially in the basal plane, while the $Ir(CO)_9L_3$ clusters exhibit a mixture of axial and radical substitution so the L are inequivalent. Unfortunately, the electronic and steric consequences of the differing substitution pattern are difficult to predict. It should be noted that the role of bridging CO groups in enhancing CO dissociation has been questioned by Poë[12b-d] since the $Ir_4(CO)_{12-n}[P(OPh)_3]_n$ and $Ir_4(CO)_{12-n}(AsPh_3)_n$ clusters show only a small (5- to 20-fold) rate enhancement on introduction of a bridging CO group.

The similarity between the k_1 rates of $Ir_4(CO)_{12}$ and $Ir_4(CO)_9[HC(PPh_2)_3]$ is not mirrored in the k_2 rates for these clusters. Thus with $P(n\text{-}Bu)_3$, $Ir_4(CO)_{12}$[12] ($k_2 = 1.4 \times 10^{-2}$ M^{-1} s^{-1}, chlorobenzene solvent) reacts about 1000 times faster than $Ir_4(CO)_9[HC(PPh_2)_3]$ ($k_2 = 1.01 \times 10^{-5}$ M^{-1} s^{-1}, DME solvent) at 40 °C. If attack occurs at the apical position in $Ir_4(CO)_9[HC(PPh_2)_3]$ then, neglecting all other effects, $Ir_4(CO)_{12}$ would statistically be expected to react four times faster than $Ir_4(CO)_9[HC(PPh_2)_3]$ as it has four equivalent $Ir(CO)_3$ groups. Compensating for this statistical effect still leaves $Ir_4(CO)_{12}$ reacting about 250 times faster than $Ir_4(CO)_9[HC(PPh_2)_3]$. In the solid-state structures[16,17] the average iridium–carbonyl bond is shortened by 0.08 Å in $Ir_4(CO)_9[HC(PPh_2)_3]$ (Table XV). The average basal Ir–Ir bond length in $Ir_4(CO)_9[HC(PPh_2)_3]$ is about the same as the average Ir–Ir bond length in $Ir_4(CO)_{12}$, but the average apical-basal Ir–Ir bond length in $Ir_4(CO)_{12}$ is shortened by 0.01 Å. Intrinsically, we expect that $Ir_4(CO)_9[HC(PPh_2)_3]$ should be less prone to nucleophilic attack compared to $Ir_4(CO)_{12}$ because of the greater electron donating and lower π acceptor ability of phosphines over carbonyls. It also seems reasonable that the effect on k_2 should be greater than for the k_1 process, since nucleophilic attack should depend critically on the electron density in the cluster.

It is more difficult to assess the relative k_2 values for the intermediate $Ir_4(CO)_{12-x}L_x$ ($x = 1, 2$) clusters. Rate data are scarce, as these reactions proceed via primarily CO dissociative processes. Both $Ir_4(CO)_{12}$ and $Ir_4(CO)_9[HC(PPh_2)_3]$ have T_d carbonyl configurations. Monodentate phosphine ligand substituted $Ir_4(CO)_{12-x}L_x$ clusters have edge bridging carbonyl groups and the site of ligand attack is not known for these species. Rate constants can be estimated from the reported[18] k_{obs} at 89 °C, for the associative term of the reaction of $Ir_4(CO)_{10}[P(OPh)_3]_2$ with $P(n\text{-}Bu)_3$, and by using k_2 values for $Ir_4(CO)_{12}$ and $Ir_4(CO)_9[HC(PPh_2)_3]$ estimated at 89 °C from the activation parameters. The relative values are shown in eq 13; the upper values are uncorrected

$$Ir_4(CO)_{12} \xrightarrow[375]{1.5 \times 10^3} Ir_4(CO)_{10}[P(OPh)_3]_2 \xrightarrow[155]{3.1 \times 10^2} Ir_4(CO)_9[HC(PPh_2)_3] \xrightarrow[1.0]{1.0} \quad (13)$$

and the lower values have been statistically adjusted to represent four sites of attack (i.e. $Ir(CO)_3$ fragments) in $Ir_4(CO)_{12}$, two sites of attack in $Ir_4(CO)_{10}[P(OPh)_3]_2$, and one site of attack for $Ir_4(CO)_9[HC(PPh_2)_3]$. Even when corrected for decreasing the number of sites available for nucleophilic attack the ligand-dependent rates decrease for the $Ir_4(CO)_{12}$ clusters on phosphorus ligand substitution. Thus, for the k_2 path there is no unusual effect of bridging CO ligands ($Ir_4(CO)_{10}(PPh_3)_2$ contains bridging CO's and the others do not) on the reaction rate.

The relative k_1 and k_2 values for stepwise substitution of CO by PPh_3 on $Rh_4(CO)_{12-x}[PPh_3]_x$ clusters can be better compared. For $x = 3$, the $HC(PPh_2)_3$ ligand data are used. Equation 14

$$Rh_4(CO)_{12} \xrightarrow{1.0} Rh_4(CO)_{11}(PPh_3) \xrightarrow{6.2 \times 10^{-3}} Rh_4(CO)_{10}(PPh_3)_2 \xrightarrow{1.3 \times 10^{-4}} Rh_4(CO)_9[HC(PPh_2)_3] \xrightarrow{2.3 \times 10^{-3}} \quad (14)$$

illustrates the relative k_1 values and eq 15 the relative k_2 values at 28 °C. All data are from chlorobenzene solvent except for

$$Rh_4(CO)_{12} \xrightarrow{1.0} Rh_4(CO)_{11}(PPh_3) \xrightarrow{2.2 \times 10^{-2}} Rh_4(CO)_{10}(PPh_3)_2 \xrightarrow{1.0 \times 10^{-5}} Rh_4(CO)_9[HC(PPh_2)_3] \xrightarrow{1.2 \times 10^{-5}} \quad (15)$$

(15) Karel, K. J.; Norton, J. R. *J. Am. Chem. Soc.* **1974**, *96*, 6812.
(16) Churchill, M. R.; Hutchinson, J. P. *Inorg. Chem.* **1978**, *17*, 3528.
(17) Huq, R.; Poë, A. J. *J. Organomet. Chem.* **1982**, *226*, 277.
(18) Sonnenberger, D. C.; Atwood, J. D. *Organometallics* **1982**, *1*, 694.

$Rh_4(CO)_9[HC(PPh_2)_3]$, which is reported for measurements in CH_2Cl_2 solvent for the k_2 terms. First consider the behavior of the k_1 term as the degree of phosphine substitution increases. If the site of CO dissociation is from the apical position in $Rh_4(CO)_9[HC(PPh_2)_3]$, as it seems to be in $Ir_4(CO)_9[HC(PPh_2)_3]$ and $Co_4(CO)_9[HC(PPh_2)_3]$ (vide supra), then the steric interaction between the dissociating carbonyl and the phosphine ligands of $HC(PPh_2)_3$ is expected to be small. From this, one might conclude a large intracluster electronic effect of the phosphine ligands in $Rh_4(CO)_9[HC(PPh_2)_3]$ compared to $Rh_4(CO)_{12}$, much larger than found with iridium. For $Ir_4(CO)_{12}$ and $Ir_4(CO)_9[HC(PPh_2)_3]$ a reasonable comparison can be made for they both have T_d carbonyl configurations and the apical position in $Ir_4(CO)_9[HC(PPh_2)_3]$ is similar to any one of four apical positions in $Ir_4(CO)_{12}$. The cluster $Rh_4(CO)_{12}$ has a C_{3v} carbonyl configuration and the site of carbonyl loss is not known on this cluster (or any $Rh_4(CO)_{12-x}L_x$ cluster). Only if the apical position in $Rh_4(CO)_{12}$ lost CO would a comparison with $Rh_4(CO)_9[HC(PPh_2)_3]$ be reasonable. However, because the CO dissociative rates are so drastically different, this might imply that the mechanisms differ and the site of CO dissociation for $Rh_4(CO)_{12}$ occurs from a basal metal and not the apical position.

Comparison of the k_2 terms for the CO substitution by PPh_3 on $Rh_4(CO)_{12-x}(PPh_3)_x$ and $Rh_4(CO)_9[HC(PPh_2)_3]$ is difficult, because the site(s) of nucleophilic attack on $Rh_4(CO)_{12-x}(PPh_3)_x$ is not known. Metal centers already bound to a phosphine ligand probably are not subject to attack and it is reasonable to presume the site of attack on $Rh_4(CO)_9[HC(PPh_2)_3]$ is the apical position. The ultimate site(s) of CO loss on any of the clusters is not known. The rate of associative attack on $Rh_4(CO)_9[HC(PPh_2)_3]$ is much slower than for $Rh_4(CO)_{12}$. Both clusters have a C_{3v} carbonyl configuration, but the PPh_3 ligand is in the apical position in $Rh_4(CO)_8[HC(PPh_2)_3](PPh_3)$ and in a basal-axial position in $Rh_4(CO)_{11}(PPh_3)$. The $HC(PPh_2)_3$ ligand does not sterically interact with the apical position and so neither cluster is subject to phosphine ligand steric effects at the site of attack. Even with a 1/4 statistical adjustment (assuming all four rhodium centers are available for ligand attack) the rate with $Rh_4(CO)_{12}$ is about 10^4 times greater than with $Rh_4(CO)_9[HC(PPh_2)_3]$. This same relative behavior was seen between $Ir_4(CO)_{12}$ and $Ir_4(CO)_9[HC(PPh_2)_3]$ in associative reactions with $P(n\text{-}Bu)_3$ or $P(OMe)_3$. This implies, as with iridium, the difference in the k_2 terms between $Rh_4(CO)_{12}$ and $Rh_4(CO)_9[HC(PPh_2)_3]$ arises from a change in the electronic nature of the cluster. Increased electron density on Rh in the phosphine-substituted species should make it a poorer electrophile for associative attack.

The effect of degree of phosphine ligand substitution on the $Co_4(CO)_{12-x}L_x$ clusters for the CO dissociative, k_1, term has been previously reported.[6,19-21] These studies concluded that the k_1 term depends on the nature of the substituent ligand L but is independent of the degree of phosphine substitution at the axial sites on the Co_4 unit. This contrasts to the behavior of both rhodium and iridium clusters and means all three metals show different effects on the k_1 term as the degree of phosphine substitution increases. The relative ordering for the k_2 term is $Co_4(CO)_{11}[P(OMe)_3] \gg Co_4(CO)_9[HC(PPh_2)_3] > Co_4(CO)_9[P(OMe)_3]_3 > Co_4(CO)_{10}[P(OMe)_3]_2$.

Conclusions. These studies show the $M_4(CO)_9[HC(PPh_2)_3]$ clusters (M = Co, Rh, Ir) exhibit increased reactivity toward CO dissociation in the order Ir $\ll$ Co < Rh with ratios of 10^{-5}:1:667. The dramatic decrease in reactivity in the Ir complex can be attributed to the absence of bridging carbonyls. Enhanced lability of CO bridged clusters toward CO dissociation may explain the series Os $\ll$ Ru < Fe observed for CO dissociation in the $M_3(CO)_{12}$ clusters.[3a,b] Only $Fe_3(CO)_{12}$ contains bridging CO groups. Phosphine substitution for CO at metal atoms removed from the site of CO dissociation produces small to modest decreases in the rate of CO dissociation as long as the number of bridging carbonyls does not change. Our data for $Ir_4(CO)_9$(tripod) and earlier data[15] for substitution in $Ir_4(CO)_{12}$ and $Ir_4(CO)_9(PPh_3)_3$ suggest that bridging carbonyl groups may enhance cluster lability as originally suggested by Norton and Collman.[22] However, the 10^4 increase occurs in CO dissociation rates. Associative attack shows no special enhancement. Given the superior electron acceptor ability of a bridging CO vs a terminal CO group in these clusters[5] their presence might stabilize the excess dπ electron density, which develops in the cluster as a π-acceptor CO ligand dissociates. The presence of bridging CO groups should also weaken the π-backbonding to the terminal CO groups, which could result in enhanced dissociative lability. In Scheme I we depict how a doubly-bridging CO group can easily move to a triply-bridging position and also relieve electronic deficiency in a σ-acceptor metal orbital on dissociation of an apical terminal CO group. For associative attack a primary concern should be the presence of a suitable metal localized σ-acceptor orbital as considered below.

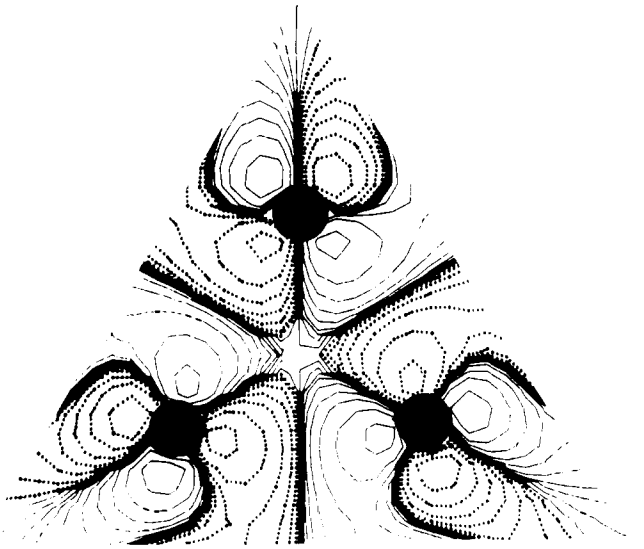

Figure 10. Lowest unoccupied metal–metal antibonding orbital characteristic of a triangular array of metal atoms. Taken from SCF–Xα–DV calculations[24] for $Ru_3(CO)_{12}$.

A striking difference between the reactivity of mononuclear transition-metal carbonyls or phosphine-substituted carbonyls and the cluster systems described here is the presence of a facile associative path for CO substitution in the latter compounds. A dinuclear structure does not seem to be sufficient for introducing an associative mechanism since $M_2(CO)_{10}$ (M = Mn, Re) and $Co_2(CO)_8$ react predominantly by CO dissociative or radical paths.[13b] For $Rh_4(CO)_{12}$ and $Rh_4(CO)_9[HC(PPh_2)_3]$ the associative lability is so high that stopped-flow or low-temperature methods must be used to monitor the kinetic processes. Whether bridging CO groups are present or not does not appear to be as important a factor in controlling the rate of associative CO substitution. In a relative sense the associative path becomes dominant as one descends the periodic table. This could arise from increased steric accessibility for nucleophilic attack as cluster size increases, as well as from the decreased tendency to CO bridging, which favors the dissociative path. For the $M_4(CO)_9[HC(PPh_2)_3]$ series associative rates of substitution increase in the order Ir < Co $\ll$ Rh with ratios of 10^{-3}:1:10^6. Phosphine substitution of CO groups in the cluster generally leads to a decrease in associative substitution reactions because of increased electron density (decreased electrophilicity). The magnitude of this decrease is not as pronounced as in mononuclear systems. In a few systems phosphine substitution can enhance CO substitution, as noted for $Ir_4(CO)_{12-n}[P(n\text{-}Bu)_3]_n$ or $M_3(CO)_{12-n}[P(n\text{-}Bu)_3]_n$ (n = 0, 1, M = Os, Ru).[12,23]

(19) Darensbourg, D. J.; Peterson, B. S.; Schmidt, R. E., Jr. *Organometallics* **1982**, *1*, 306.
(20) Darensbourg, D. J.; Incorvia, M. J. *J. Organomet. Chem.* **1979**, *171*, 89.
(21) Darensbourg, D. J.; Incorvia, M. J. *Inorg. Chem.* **1980**, *19*, 2585.
(22) Norton, J. R.; Collman, J. P. *Inorg. Chem.* **1973**, *12*, 476.
(23) Brodie, N. M. J.; Poë, A. J.; Sekhar, V. *J. Chem. Soc., Chem. Commun.* **1985**, 1090.

For the origin of the nucleophilic substitution path, which seems common in trinuclear and higher metal clusters,[13b] we offer the following speculation. As found for organometallic radicals[24] a key requirement for the existence of such a path is a suitable acceptor orbital on the metal. When triangular faces of metal atoms occur, then the lowest lying metal localized acceptor orbital is the σ^* orbital for the cyclopropane-like σ bonding network as found in $Ru_3(CO)_{12}$.[25] This orbital is directed out the edge of the cluster as shown in Figure 10 and may be accessible to attack by a nucleophile. In Table XIV we collect several properties relevant to this discussion. The energy of the lowest acceptor orbital follows the order $Co_4 < Rh_4 < Ir_4$ as inferred from optical spectroscopy, and the electrochemical reduction potential measurements, E_{pc}, support this trend. Electrophilic character at the metal as reflected by the cluster core charge calculated by SCF-Xα-DV theory,[5] $\int \rho$, or by the amount of charge donated to the CO ligands, ν(CO), should increase as $Co_4 < Rh_4 \sim Ir_4$. Metal-carbonyl bond strengths inferred from both length data, M-C^{ap}, or from the trend in rates of dissociative CO loss discussed earlier appear to follow the order Rh < Co < Ir. Steric accessibility for nucleophilic attack should also parallel the metal-metal bond lengths, M^{ap}-M^{bas} Co $\ll$ Ir $\sim$ Rh. Poë and co-workers[3b,12] have emphasized that a weakened metal-metal bond should enhance the susceptibility of clusters to associative attack because metal ligand bonding in the associative transition state will reduce the number of electrons involved in cluster bonding. All these factors, some operating in opposition, probably contribute to determining the observed trend in k_2.

Acknowledgment. This material is based on work supported by the National Science Foundation (Grants CHE-85-04088 and CHE-85-14366). We thank Johnson-Matthey, Inc. for a loan of precious metals. The insightful comments of Professor A. J. Poë are gratefully acknowledged.

Supplementary Material Available: Tables of IR carbonyl stretching frequencies, electronic absorption spectral data, anisotropic temperature factors, bond distances and angles, and hydrogen coordinates (14 pages); listing of structure factors (46 pages). Ordering information is given on any current masthead page.

(24) Trogler, W. C. *Int. J. Chem. Kinet.* **1987**, *19*, 1025.
(25) Delley, B.; Manning, M. C.; Ellis, D. E.; Berkowitz, J.; Trogler, W. C. *Inorg. Chem.* **1982**, *21*, 2247.

Stopped-Flow Kinetic Study of the Reaction of $(P(C_6H_{11})_3)_2W(CO)_3(L)$ (L = H_2, D_2, and N_2) with Pyridine. Kinetic Resolution of Reaction of Dihydride versus Molecular Hydrogen Complexes

Kai Zhang, Alberto A. Gonzalez, and Carl D. Hoff*

Contribution from the Department of Chemistry, University of Miami, Coral Gables, Florida 33124. *Received September 14, 1988*

Abstract: The rates of reaction of $(P(C_6H_{11})_3)_2W(CO)_3(L)$ (L = H_2, D_2, and N_2) with pyridine have been studied by stopped-flow kinetics. The molecular nitrogen system shows simple first-order loss of N_2 with a rate constant of 75 s^{-1} at 25 °C and an activation energy of 17.8 ± 0.7 kcal/mol. The rate of reaction of the intermediate $(P(C_6H_{11})_3)_2W(CO)_3$ with N_2 gas is 5.0 ± 1.0 × 10^5 M^{-1} s^{-1} at 25 °C in toluene solution. Reactions of the hydrogen and deuterium complexes are complicated due to the presence of both molecular hydrogen (deuterium) and dihydride (dideuteride) complexes. These data are resolved and interpreted in terms of a rapid loss of molecular hydrogen (k = 469 s^{-1} for H_2 and 267 s^{-1} for D_2 at 25 °C, $\Delta H^{\ddagger}$ = 16.9 ± 2.2 kcal/mol for H_2 and 16.2 ± 1.1 kcal/mol for D_2). The hydride complex, which is present in ~30%, reacts an order of magnitude slower than the molecular hydrogen complex (k = 37 s^{-1} for H_2 and 33 s^{-1} for D_2 at 25 °C), $\Delta H^{\ddagger}$ = 14.4 ± 0.5 kcal/mol for H_2 and 14.7 ± 0.8 kcal/mol for D_2). The rate of addition of H_2 to $(P(C_6H_{11})_3)_2W(CO)_3$ is calculated to be 2.2 ± 0.3 × 10^6 M^{-1} s^{-1} at 25 °C. These data are combined with earlier thermodynamic measurements to generate a reaction profile for binding and oxidative addition of hydrogen to the complex $(P(C_6H_{11})_3)_2W(CO)_3$.

Oxidative addition of H_2 gas is one of the fundamental steps in a number of catalytic processes. It has only recently been recognized that H_2 can coordinate as a molecule,[1] and that such complexes may be precursors to oxidative addition as depicted generally in eq 1. A number of catalytic studies have measured

$$M + H_2 \rightarrow M{-}(H_2) \rightarrow \underset{\displaystyle H}{\overset{\displaystyle |}{M{-}H}} \qquad (1)$$

the rate of uptake of hydrogen gas, but relatively few direct measurements of the rate of reaction with hydrogen have been made. In general, metal fragments that will add H_2 are highly reactive and have only transitory existence. The majority of these systems have been studied by flash photolysis.[2,3] A good example[4-11] of these systems is reaction of $Cr(CO)_6$ as described in reaction 2. The initially formed $Cr(CO)_5$ reacts on the picosecond

$$Cr(CO)_6 \xrightarrow{h\nu} Cr(CO)_5 \xrightarrow{a} Cr(CO)_5(C_6H_{12}) \xrightarrow{b} Cr(CO)_5(H_2) \qquad (2)$$

time scale to form $Cr(CO)_5$(cyclohexane). This complex contains

(1) Kubas, G. J. *Acc. Chem. Res.* **1988**, *21*, 120, and references therein.
(2) Poliakoff, M.; Weitz, E. *Adv. Organometal. Chem.* **1986**, *25*, 277.
(3) Weitz, E. *J. phys. Chem.* **1987**, *91*, 3945.
(4) Kelly, J. M.; Bent, D. V.; Hermann, H.; Schulte-Frohlinde, D.; Von Gustorf, K. E. *J. Organometal. Chem.* **1974**, *69*, 259.
(5) Lees, A. J.; Adamson, A. W. *Inorg. Chem.* **1981**, *20*, 4381.
(6) Welch, J. A.; Peters, K. S.; Vaida, V. *J. Phys. Chem.* **1982**, *86*, 1941.
(7) Hermann, H.; Grevels, F.-W.; Henne, A.; Schaffner, K. *J. Phys. Chem.* **1982**, *86*, 5151.
(8) Church, S. P.; Grevels, F.-W.; Hermann, H.; Schaffner, K. *Inorg. Chem.* **1984**, *23*, 3830.
(9) Church, S. P.; Grevels, F.-W.; Hermann, H.; Schaffner, K. *Inorg. Chem.* **1985**, *24*, 418.
(10) Church, S. P.; Grevels, F.-W.; Hermann, H.; Schaffner, K. *J. Chem. Soc., Chem. Commun.* **1985**, 30.
(11) Simon, J. D.; Xiaoliang, X. *J. Phys. Chem.* **1987**, *91*, 5538.

0002-7863/89/1511-3627$01.50/0